A SURVEY OF BOUNDARY ELEMENT METHODS FOR A TWO-DIMENSIONAL FRACTURE MODEL

By

Douglas L. James

B. Sc. (Applied Math) University of Western Ontario, 1995

A THESIS SUBMITTED IN PARTIAL FULFILLMENT OF
THE REQUIREMENTS FOR THE DEGREE OF
MASTER OF SCIENCE

in

THE FACULTY OF GRADUATE STUDIES
INSTITUTE OF APPLIED MATHEMATICS
DEPARTMENT OF MATHEMATICS

We accept this thesis as conforming
to the required standard

THE UNIVERSITY OF BRITISH COLUMBIA

September 1997

In presenting this thesis in partial fulfilment of the requirements for an advanced degree at the University of British Columbia, I agree that the Library shall make it freely available for reference and study. I further agree that permission for extensive copying of this thesis for scholarly purposes may be granted by the head of my department or by his or her representatives. It is understood that copying or publication of this thesis for financial gain shall not be allowed without my written permission.

Department of MATHEMATICS

The University of British Columbia
Vancouver, Canada

Date SEPT. 11, 1997

DE-6 (2/88)

Abstract

This thesis surveys boundary element methods for solving a two-dimensional pressurized line crack problem in a homogeneous infinite elastic medium.

Starting with an overview of linear elastic fracture mechanics, the exact solution to the pressurized line crack problem is stated and results for several pressure distributions are provided. Various numerical methods for solving the crack problem are then introduced, such as the displacement discontinuity method (DDM) using point collocation and a Galerkin method. Crack tip elements and higher-order DDM are discussed. Self-effect correction methods, stated and developed for the piecewise constant DDM on a uniform grid, are shown to significantly improve the numerical solution. An accurate DDM correction for modelling crack tip element extensions is also presented. Finally, numerical results for the various methods are given and stress intensity factors are also presented for comparison.

Table of Contents

List of Tables

List of Figures

Acknowledgements

I would first like to thank Dr. Anthony Peirce for being such an enthusiastic and insightful supervisor. I have enjoyed my many discussions with him. This work could not have been completed without his encouragement.

Next I would like to thank my friends and family for their love and support during the last year.

Finally, I would like to thank NSERC for its financial support of this and other work.

Chapter 1

Introduction

Fracture mechanics has undergone considerable development in the last 20 years. In partiuclar the field has seen the development of sophisticated nonlinear and dynamic fracture theories for various media. Nevertheless, the classical theory of linear elastic fracture mechanics (LEFM) continues to provide a useful approximation for the modelling of fractures in such materials as brittle rock. The equations of linear elasticity that arise in the context of LEFM may be numerically approximated using boundary element methods (BEM).

The discretized BEM equations result in a dense system of linear equations that has dimensions proportional to the number of boundary elements used. Therefore considerable computational effort is required to solve systems involving many boundary elements. The use of simple boundary elements with error correction techniques and fast-solution techniques or higher-order boundary elements are common ways of achieving more accurate and efficient solutions.

The following thesis will provide an overview of a few BEM solution techniques by way of their application to the analytically solvable problem of a pressurized line crack in an infinite elastic medium. The simple fracture problem will serve as a model problem to illustrate and compare the numerical methods and also to provide a test case for which numerical correction strategies may be developed. It is hoped that the results may provide guidance for numerical methods used in more

complicated problems, e.g., problems with more complicated crack geometries or inhomogeneous media.

In Chapter 2 LEFM will be introduced and its relation to the pressurized line crack problem discussed. The exact solution to the pressurized line crack problem along with asymptotic relations near the crack tip and their relationship to stress intensity factors are given. Crack width solutions are provided for various commonly used pressure distributions. Expressions for strain energy and strain energy release rates are stated.

In Chapter 3 the BEM referred to as the displacement discontinuity method (DDM) is described and its application to the line crack problem is discussed. Constant and higher-order displacement discontinuity elements (DDE) are introduced along with crack tip elements. Strain energy calculations and approaches for calculating the stress intensity factors are discussed. Tip correction strategies are introduced for constant DDE on a constant grid. In particular, tip self-effect corrections which allow high accuracy at the crack tip or the middle of the crack are numerically obtained. Also, a nearest neighbour crack tip influence coefficient correction for describing cracks that are longer than an integral multiple of the uniform grid spacing is constructed.

In Chapter 4 a Galerkin BEM formulation of the line crack problem is introduced. The Galerkin method will be provided for comparison with the DDM since one method is often preferred over the other [28]. A crack tip correction for the Galerkin method as well as strain energy calculations are also provided.

In Chapter 5 numerical results and comparisons for the methods contained in Chapters 3 and 4 are presented. The DDM and Galerkin results are compared and the accuracy of the various constant DDE correction strategies are presented. Stress intensity factors are calculated using many of the methods.

This thesis also contains several Appendices. The first of these, Appendix A, provides expressions for the stresses and displacements that accompany a general higher-order functional variation DDE. Appendix B contains a DDM matrix simplification for the symmetric pressurized crack problem. Appendix C details the construction of the matrix equations for the piecewise linear collocation DDM. The matrices constructed for the Galerkin method in Chapter 4 are calculated in Appendices D and E.

Chapter 2

Linear Elastic Fracture Mechanics (LEFM)

LEFM has proven to be a successful theory for many fracture problems in elastic solids and brittle materials such as rock. LEFM analysis is an idealization of the crack problem in a number of ways: the crack is assumed to lie in an infinite plane; the fracturing material is assumed to form a continuum with no distinct local material microstructure; nonlinear or plastic elasticity effects occur on such a small scale so as to be negligible. The last point is a significant idealization since, in the neighbourhood of a crack tip, linear elastic theory predicts the existence of a singular stress field. The singular stress field is accompanied by the presence of a plastic process zone of nonlinear behaviour ahead of the crack tip. While a stress singularity implies that the material will be forced to yield in a nonlinear fashion, the linear solution is useful in rock mechanics as long as the criterion for small scale yield (SSY) is satisfied (see [37], p157). SSY essentially requires that the size of the plastic zone is sufficiently small with respect to the characteristic dimensions of the crack, e.g., length, thickness, specimen size. In brittle rock, the size of the process zone is related to microcracking at the crack tip and is best estimated using by a maximum normal tensile stress criterion than more classical yield criterion, such as the Von Mises criterion ([29]). The following sections provide an overview

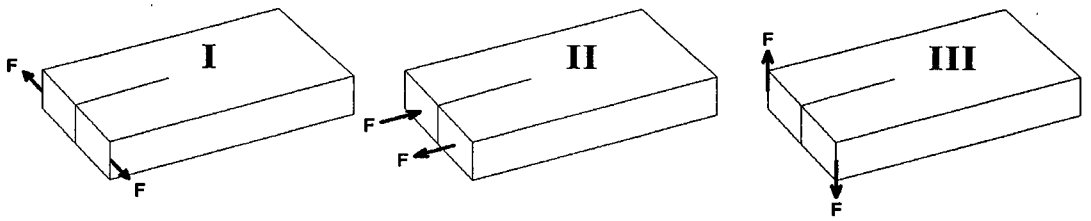

Figure 2.1: Three principle modes of fracture with accompanying forces F.

of LEFM sufficient for the development of the numerical methods that follow.

Crack Tip Loading and Modes of Displacement

Consider an infinite plate containing a crack and also having far-field tractions. Three different ways of loading the plate, designated by modes I, II and III, are illustrated in Fig. 2.1. Mode I is the "opening mode" that results from tensile stress perpendicular to the plane of the crack. Mode II is the "sliding mode" that results from in-plane shear forces. Mode III is called the "tearing mode" and is accompanied by out-of-plane shear forces. The crack is assumed to be slit-like, of length $2L$, and to lie on the line $\{(x, y)| - L \leq x \leq L, y = 0\}$. Furthermore, the crack surfaces are assumed to be traction-free. By considering uniform far field stresses which correspond to each of modes I, II and III, a plane strain elasticity problem has been formulated.

Asymptotic Crack Tip Solutions and Stress Intensity Factors

The plane strain elasticity problem of the previous subsection may be solved using Westergaard functions (see [30], [22]) or Goursat-Muskhelishvili potential functions [20]. The mode I asymptotic stress solutions for both plane stress and plane strain are

$$\begin{aligned}
\sigma_{xx} &\sim \tfrac{K_I}{\sqrt{2\pi r}} \cos(\tfrac{\theta}{2}) \left\{1 - \sin\left(\tfrac{\theta}{2}\right) \sin\left(\tfrac{3\theta}{2}\right)\right\} \\
\sigma_{yy} &\sim \tfrac{K_I}{\sqrt{2\pi r}} \cos(\tfrac{\theta}{2}) \left\{1 + \sin\left(\tfrac{\theta}{2}\right) \sin\left(\tfrac{3\theta}{2}\right)\right\} \\
\sigma_{xy} &\sim \tfrac{K_I}{\sqrt{2\pi r}} \cos(\tfrac{\theta}{2}) \sin\left(\tfrac{\theta}{2}\right) \sin\left(\tfrac{3\theta}{2}\right)
\end{aligned} \tag{2.1}$$

as $r \to 0$, where K_I is called the mode I stress intensity factor. For a remotely applied uniform tensile traction σ_∞, the stress intensity factor is

$$K_I = \sigma_\infty \sqrt{\pi a}. \tag{2.2}$$

The asymptotic displacement fields in the neighbourhood of the crack tip are found to be

$$\begin{aligned}
u_x &\sim \tfrac{K_I}{2G} \sqrt{\tfrac{r}{2\pi}} \cos\left(\tfrac{\theta}{2}\right) \left\{\kappa - 1 + 2\sin^2\left(\tfrac{\theta}{2}\right)\right\} \\
u_y &\sim \tfrac{K_I}{2G} \sqrt{\tfrac{r}{2\pi}} \sin\left(\tfrac{\theta}{2}\right) \left\{\kappa + 1 - 2\cos^2\left(\tfrac{\theta}{2}\right)\right\}
\end{aligned} \tag{2.3}$$

as $r \to 0$, where

$$\kappa = \begin{cases} \frac{3-\nu}{1+\nu}, & \text{plane stress} \\ 3 - 4\nu, & \text{plane strain} \end{cases} \tag{2.4}$$

and ν is Poisson's ratio [18]. Inside the crack, along the $\theta = \pi$ line, the asymptotic form for the normal displacement is

$$u_y \sim \frac{K_I}{2G} \sqrt{\frac{r}{2\pi}} \{4(1-\nu)\} = \frac{4K_I}{E'} \sqrt{\frac{r}{2\pi}} \qquad \text{(plane strain)}. \tag{2.5}$$

The solutions for modes II and III have the same asymptotic r dependence (see [35] for details) and can be derived in a similar way. In fact, many of the problems of LEFM can be solved using similar techniques since they also involve plane elasticity problems. N. I. Muskhelishvili [20] has developed a general method for solving plane elasticity problems through a complex variable mapping scheme and use of the Kolosov equations. Brief introductions to the technique can be found in [34] and [32].

As (2.1) indicates, the strength of the stress singularity in the neighbourhood of the crack tip is controlled by the stress intensity factor, K_I. As a result, the stress intensity factor plays an important role in LEFM for predicting when a solid will yield and crack elongation will occur. A simple criterion for deciding when the crack will propagate is whether or not the stress intensity factor is greater than a critical stress intensity value, K_{IC}, e.g.,

$$K_I \geq K_{IC}\,. \tag{2.6}$$

This concept was first studied by Griffith ([16], [17]) and is often called Griffith's stability criterion. This and other fracture propagation criteria can be interpreted as conditions on the energy release rate in order for the crack to open, e.g., see (2.29). More detailed discussions of dynamic fracture are given by Kanninen and Popelar [18] or Freund [13].

Pressurized Line Crack

The two-dimensional line crack problem for a solid in equilibrium is important for the study of fracture mechanics. In this case, it is possible to obtain closed form solutions with relative ease compared to fractures of a more complicated geometry. While the growth of cracks is inherently a dynamic phenomena, an understanding of the equilibrium case is a natural starting point. Also, the simple line crack problem in an elastic medium provides a test bed for developing more sophisticated numerical methods for fracture mechanics.

First studied by Griffith [16] in 1920, the pressurized line crack problem consists of a line crack (or hollow slit) of length $2L$, situated along the x axis and centred about the origin (see Fig. 2.2). The problem is assumed to be symmetric about the x and y axes and situated in an infinite plane. The stresses in the medium are

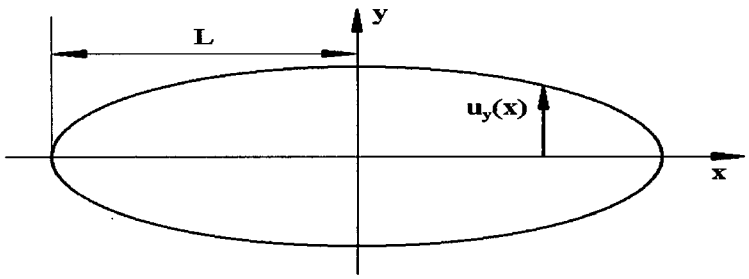

Figure 2.2: Pressurized line crack

given by $\sigma_{xx}(x,y)$, $\sigma_{yy}(x,y)$ and $\sigma_{xy}(x,y) = \sigma_{yx}(x,y)$. The crack interface located in the $y > 0$ region is called the upper crack face, and the displacement of the upper crack face is given by $u_y(x) = u_y(x,0)$. The elasticity boundary conditions for the $x \geq 0$ upper crack face are

$$\begin{aligned} \sigma_{yy}(x,0) &= -p(x), \quad 0 \leq x \leq L, \\ \sigma_{xy}(x,0) &= 0, \qquad\quad x \geq 0, \\ u_y(x) \quad &= 0, \qquad\quad x \geq L, \end{aligned} \tag{2.7}$$

where $p(x)$ is an even function representing the net pressure responsible for holding open the crack. An additional boundary condition is that all stresses are zero an infinite distance from the crack. This problem will be referred to as the symmetric crack problem.

Displacement and Stress Solution

The symmetric crack problem has been solved using the plane elasticity solution techniques developed by Muskhelishvili [20], e.g., England and Green [11], Green and Zerna [15] or Sneddon [31]. The normal displacement of the upper crack face is

$$u_y(x) = -\frac{4}{\pi E'} \int_x^L \frac{\xi g(\xi) d\xi}{\sqrt{x^2 - \xi^2}}, \qquad 0 \leq x \leq L, \tag{2.8}$$

and the stress ahead of the crack tip is given by

$$\sigma_{yy}(x,0) = \frac{2}{\pi}\left[\frac{xg(L)}{\sqrt{x^2-L^2}} - g(0) - x\int_0^L \frac{g'(\xi)d\xi}{\sqrt{x^2-\xi^2}}\right], \qquad x \geq L, \tag{2.9}$$

where

$$g(\xi) = \int_0^\xi \frac{p(x)dx}{\sqrt{\xi^2-x^2}}, \qquad 0 \leq x \leq L. \tag{2.10}$$

The plane strain modulus, E', can also be expressed in terms of Young's modulus, E, the shear modulus, G, and Poisson's ratio, ν, as

$$E' = \frac{E}{1-\nu^2} = \frac{2G}{1-\nu}. \tag{2.11}$$

These crack results were derived for the case in which $g(\xi)$ is differentiable. Note that if $p(x)$ is differentiable then $g(\xi)$ is a continuous function. It turns out [31] that (2.8) and (2.9) are valid even if $p(x)$ has a finite number of jump discontinuities. The stress in the x-direction is given by the equations of plane strain as

$$\sigma_{xx}(x,0) = \sigma_{yy}(x,0), \qquad x > L. \tag{2.12}$$

It can also be verified that the condition $\sigma_{xy}(x,0) = 0$ is satisfied for $x \geq 0$. An alternate expression of $u_y(x)$ is given by Spence and Sharp [33, appendix A] as

$$u_y(x) = -\frac{2}{\pi E'}\int_0^L \ln\left|\frac{\sqrt{L^2-x^2}-\sqrt{L^2-\xi^2}}{\sqrt{L^2-x^2}+\sqrt{L^2-\xi^2}}\right| p(\xi)d\xi\,. \tag{2.13}$$

Alternatively, the solution to the crack elasticity problem may express the pressure in terms of the crack width. Spence and Sharp [33, see Appendix A] have shown that the crack solution may be written as

$$p(x) = \frac{E'}{4\pi}\text{p.v.}\int_{-L}^L \frac{du_y(s)}{ds}\frac{ds}{s-x}, \tag{2.14}$$

where p.v. denotes the Cauchy principle value. For the symmetric problem, (2.14) simplifies to

$$p(x) = -\frac{E'}{\pi}\int_0^L \frac{du_y(s)}{ds}\frac{s}{s^2-x^2}ds \tag{2.15}$$

where the principle value is assumed. Integration by parts and the condition $u_y(L) = 0$ yields

$$p(x) = -\frac{E'}{\pi}\int_0^L u_y(s)\frac{s^2+x^2}{(s^2-x^2)^2}ds. \tag{2.16}$$

Both (2.15) and (2.16) will be useful for developing numerical approximation schemes to the crack stress boundary value problem.

Stress Singularities and the Stress Intensity Factor

From (2.9) it is clear that a stress singularity can exist at the crack tip, i.e., at $x = L$. An asymptotic expansion about $x = L$, assuming $g(\xi)$ is nonsingular, identifies the square-root singularity typical of LEFM:

$$\sigma_{yy}(x,0) \sim \frac{2}{\pi}\left\{\sqrt{\frac{L}{2}}g(L)\frac{1}{\sqrt{x-L}} + \left(L\int_0^L \frac{g'(\xi)d\xi}{\sqrt{L^2-\xi^2}} - g(0)\right) + O\left(\sqrt{x-L}\right)\right\}, \qquad x \to L_+. \tag{2.17}$$

The stress intensity factor, K_I, can then be defined as

$$K_I = \lim_{r\to 0+}\sqrt{2\pi r}\sigma_{yy}(L+r,0) \tag{2.18}$$

Using (2.17), K_I is found to be

$$K_I = 2\sqrt{\frac{L}{\pi}}g(L) = 2\sqrt{\frac{L}{\pi}}\int_0^L \frac{p(x)dx}{\sqrt{L^2-x^2}}. \tag{2.19}$$

From (2.19) it is clear that $g(L)$ has a direct effect on the strength of the singularity. Also, note that K_I has no dependence on material properties.

Constant Pressure Distribution Solution

By far the most popular pressure distribution in the literature is that in which the pressure is constant. In this case, the function $g(\xi)$ is also constant and given by

$$g(\xi) = \int_0^\xi \frac{p_0 dx}{\sqrt{\xi^2-x^2}} = \frac{p_0\pi}{2}, \qquad 0 < \xi < L. \tag{2.20}$$

Using (2.8), the displacement solution for the upper crack face is

$$u_y(x,0) = -\frac{4}{\pi E'}\int_x^L \frac{\xi g(\xi)d\xi}{\sqrt{x^2-\xi^2}} = \frac{2p_0}{E'}\sqrt{L^2-x^2}, \qquad 0 \le x \le L, \tag{2.21}$$

and therefore a maximum crack width of

$$w_0 = \frac{4Lp_0}{E'}, \tag{2.22}$$

occurs at the middle of the crack ($x = 0$). The stress ahead of the crack tip is given by

$$\sigma_{yy}(x,0) = p_0\left[\frac{x}{\sqrt{x^2-L^2}} - 1\right], \qquad x > L\,. \tag{2.23}$$

The stress intensity factor, determined from (2.23) using (2.18) or from (2.19), is found to be

$$K_I = p_0\sqrt{\pi L}. \tag{2.24}$$

Polynomial Pressure Distribution

If the pressure is given by a polynomial function,

$$p(x) = p_0 + p_1 x + p_2 x^2 + p_3 x^3 + ...,$$

Valkó and Economides [36] have shown that

$$g(\xi) = \frac{\pi p_0}{2} + p_1\xi + \frac{\pi p_2 \xi^2}{2} + \frac{2p_3\xi^3}{3} + ..., \tag{2.25}$$

$$\begin{aligned} u_y(x,0) \;=\; & \frac{2p_0}{E'}\sqrt{L^2-x^2} + \frac{2p_1}{\pi E'}\left[L\sqrt{L^2-x^2} + x^2\ln\left(\frac{L+\sqrt{L^2-x^2}}{x}\right)\right] + \\ & + \frac{p_2}{3E'}\left(L^2+2x^2\right)\sqrt{L^2-x^2} + \\ & + \frac{p_3}{\pi E'}\left[\left(\frac{2}{3}L^3 + Lx^2\right)\sqrt{L^2-x^2} + x^4\ln\left(\frac{L+\sqrt{L^2-x^2}}{x}\right)\right] + ... \end{aligned}$$

and

$$\sigma_{yy}(x,0) \;=\; p_0\left[\frac{x}{\sqrt{x^2-L^2}} - 1\right] + \frac{2p_1}{\pi}\left[\frac{Lx}{\sqrt{x^2-L^2}} - x\arctan\left(\frac{L}{\sqrt{x^2-L^2}}\right)\right] +$$

$$+p_2\left[\left(\frac{L^2x}{2}-x^3\right)/\sqrt{x^2-L^2}-x^2\right]+$$
$$+\frac{2p_3}{\pi}\left[\left(\frac{L^3x}{3}-Lx^3\right)/\sqrt{x^2-L^2}-x^3\arctan\left(\frac{L}{\sqrt{x^2-L^2}}\right)\right]+...$$

The mode I stress intensity factor, found by combining (2.19) and (2.25), is

$$K_I=2\sqrt{\frac{L}{\pi}}g(L)=2\sqrt{\frac{L}{\pi}}\left(\frac{\pi p_0}{2}+p_1L+\frac{\pi p_2L^2}{2}+\frac{2p_3L^3}{3}+...\right). \tag{2.26}$$

Pressure Distributions for Smoothly Closing Cracks

Understanding the crack tip region is, by nature, fundamental to understanding the fracture process. Indeed, in hydraulic fracturing the crack tip region is the source of much concern [9], [28]. A popular boundary condition, often called the Barenblatt tip condition based on the work of Barenblatt [2], is that the displacement field, u_y, satisfy the smooth closing condition

$$\frac{du_y(x=L,0)}{dx}=0$$

In order for this to occur, it is sufficient to have

$$g(L)=0 \tag{2.27}$$

which is the so-called "zipper crack equation" [36]. From (2.19) it is clear that the zipper crack equation is equivalent to having

$$K_I=0.$$

In terms of the pressure function, $p(z)$, a region of "negative pressure" is required in order to force the solid to close smoothly.

A popular pressure distribution used by Khristianovitch and Zheltov ([19], [38]), Barenblatt [2] and Geertsma and de Klerk [14] is a two-level piecewise constant function given by

$$p(x)=\begin{cases}p_1, & x\le x_0\\ -p_2, & x_0<x\le L\end{cases}$$

where x_0 is the location of the pressure discontinuity, and p_1 and p_2 are positive constants. The location of the discontinuity is determined by the zipper crack equation. Equation (2.10) implies

$$g(\xi) = \begin{cases} \frac{p_1\pi}{2}, & x \le x_0 \\ -\frac{p_2\pi}{2} + (p_1+p_2)\arctan\left[\frac{x_0}{\sqrt{\xi^2-x_0^2}}\right], & x > x_0 \end{cases}$$

and so (2.27) implies [19]

$$x_0 = L\sin\frac{\pi p_2}{2(p_1+p_2)}.$$

Strain Energy of the Line Crack

When a crack is opened, energy is stored in the elastic medium in the form of strain potential energy. Using the definition of work, the energy stored in the medium for $x > 0$, per unit thickness (in the $\hat{z}$ direction), for the symmetric crack problem is

$$W_0 = \int_0^L p(x)u_y(x)dx.$$

This result assumes that the pressure varies linearly with the displacement. Sneddon [31] showed that this may also be written in terms of $g(\xi)$ as

$$W_0 = \frac{4}{\pi E'}\int_0^L \xi\left[g(\xi)\right]^2 d\xi. \tag{2.28}$$

Taking the partial derivative of (2.28) with respect to L yields the strain energy release rate per crack length

$$\begin{aligned} \frac{\partial W_0}{\partial L} &= \frac{4L}{\pi E'}\left[g\left(L\right)\right]^2 \\ &= \frac{K_I^2}{E'} \qquad \text{(using (2.19))}, \end{aligned} \tag{2.29}$$

This last result, given by Rice in [26], will prove useful for estimating K_I numerically.

Chapter 3

The Displacement Discontinuity Method (DDM)

The displacement discontinuity method (DDM) is a boundary element method (BEM) suitable for the numerical description of cracks in a linear elastic medium. Originally developed by Crouch ([6], [7]), the DDM may be used to approximate the crack boundary by a sequence of boundary elements called displacement discontinuity elements (DDE), or DD elements. The DDE utilizes the analytic solution for a finite segment of a (constant) displacement discontinuity in an infinite solid in order to approximate the resulting tractions at the locations of other DDE on the crack. As a result, for a properly formulated elasticity problem (see Timoshenko [34]), it is possible to construct a system of equations so that the unknown normal and tangential stresses and/or displacements may be solved for in terms of the known ones [8]. The following study will be concerned with stress boundary value problems, in which the tractions are specified on the boundary and the boundary displacements are to be determined. An example of such a problem is the pressurized crack for which the pressure is specified and the crack width is to be determined. An excellent reference for the DDM, which contains much of the following material, is the text by Crouch and Starfield [8]. Numerical results for the various methods presented in this chapter will be delayed until Chapter 5.

The Displacement Discontinuity Element (DDE)

Consider the problem of a DDE in an infinite elastic solid. In this case, the displacement field, $u_j = (u_x, u_y)$, is everywhere continuous except along a finite line segment in the xy-plane. Denote the line segment by $C = \{(x,y)|\ -a \leq x \leq a,\ y = 0\}$. Since the DDE will be used to represent the displacement between two crack faces, it is useful to refer to the $y = 0_-$ side of C as the negative side and the $y = 0_+$ side of C as the positive side. While more general functional forms are possible (see p. 22), in what follows, it will be sufficient to consider the simplest and most popular case of a constant DD, i.e., the DD is constant along C. The DDE is described by the coordinates D_x and D_y, where

$$\begin{aligned} D_x &= u_x(x,0_-) - u_x(x,0_+) \\ D_y &= u_y(x,0_-) - u_y(x,0_+)\,. \end{aligned}$$

The D_x and D_y coordinates describe the DDE's normal and shear displacements, respectively, that occur upon crossing C. Note that the convention is for D_y to be negative when the crack faces are physically displaced from one another, i.e., the crack has been opened.

The resulting displacement and stress fields associated with the constant DDE were given by Crouch as

$$u_x(x,y) = D_x\left[2(1-\nu)f_{,y} - yf_{,xx}\right] + D_y\left[-(1-2\nu)f_{,x} - yf_{,xy}\right] \tag{3.1}$$

$$u_y(x,y) = D_x\left[(1-2\nu)f_{,x} - yf_{,xy}\right] + D_y\left[2(1-\nu)f_{,y} - yf_{,yy}\right] \tag{3.2}$$

and

$$\sigma_{xx}(x,y) = 2G\left\{D_x\left[2f_{,xy} + yf_{,xyy}\right] + D_y\left[f_{,yy} + yf_{,yyy}\right]\right\} \tag{3.3}$$

$$\sigma_{yy}(x,y) = 2G\left\{D_x\left[-yf_{,xyy}\right] + D_y\left[f_{,yy} - yf_{,yyy}\right]\right\} \tag{3.4}$$

$$\sigma_{xy}(x,y) = 2G\left\{D_x\left[f_{,yy} + yf_{,yyy}\right] + D_y\left[-yf_{,xyy}\right]\right\} \tag{3.5}$$

where

$$f(x,y) = \frac{-1}{4\pi(1-v)}\left[y\left(\arctan\frac{y}{x-a} - \arctan\frac{y}{x+a}\right)\right.$$
$$\left.-(x-a)\ln\sqrt{(x-a)^2+y^2} + (x+a)\ln\sqrt{(x+a)^2+y^2}\right]. \quad (3.6)$$

When constructing a linear DDM approximation of the solution to the pressurized line crack, it will be useful to know the stress resulting from a single DDE at the position of another DDE on the discretized crack. With this in mind, the displacements and stresses along the x-axis can be the calculated from (3.1)-(3.6). For $|x| > a$, $y = 0$ the displacement components are

$$u_x(x,0) = -\frac{(1-2\nu)}{4\pi(1-\nu)}\ln\left|\frac{x-a}{x+a}\right| D_y$$
$$u_y(x,0) = +\frac{(1-2\nu)}{4\pi(1-\nu)}\ln\left|\frac{x-a}{x+a}\right| D_x$$

while for $|x| < a$ they are

$$u_x(x,0_\pm) = \mp\frac{1}{2}D_x - \frac{(1-2\nu)}{4\pi(1-\nu)}\ln\left|\frac{x-a}{x+a}\right| D_y \quad (3.7)$$
$$u_y(x,0_\pm) = \mp\frac{1}{2}D_y + \frac{(1-2\nu)}{4\pi(1-\nu)}\ln\left|\frac{x-a}{x+a}\right| D_x\,. \quad (3.8)$$

The constant discontinuities D_x and D_y are clearly visible from (3.7) and (3.8) for $|x| < a$.

From (3.3)-(3.6) the stresses along y=0 are found to be

$$\sigma_{xx}(x,0) = \frac{-G}{\pi(1-\nu)}\frac{a}{x^2-a^2}D_y \quad (3.9)$$
$$\sigma_{yy}(x,0) = \frac{-G}{\pi(1-\nu)}\frac{a}{x^2-a^2}D_y \quad (3.10)$$
$$\sigma_{xy}(x,0) = \frac{-G}{\pi(1-\nu)}\frac{a}{x^2-a^2}D_x \quad (3.11)$$

with $\sigma_{xy}(x,0) = \sigma_{yx}(x,0)$. Notice that stresses are singular at the DDE's endpoints ($x = \pm a$) but continuous everywhere else. Also, the stresses are continuous across the $y = 0$ line, by construction.

DDM Solution of the Pressurized Line Crack Problem

Once again, consider the pressurized line crack problem in an infinite elastic body. The boundary conditions are

$$\begin{aligned} \sigma_{yy}(x,0) &= -p(x), \quad |x| \le L, \\ \sigma_{xy}(x,0) &= 0, \qquad -\infty < x < \infty, \\ u_y(x,0) &= 0, \qquad |x| \ge L, \end{aligned}$$

along with the additional condition that all stresses and displacements are zero at infinity.

By dividing the crack into N line segments, each representing a DDE placed end-to-end with adjacent DDE, the width of a crack may be approximated by a piecewise constant (PWC) function. Let the N DDE be denoted by (D_x^k, D_y^k), $k = 1, .., N$ and be of length $h_k = 2a_k$. The midpoint of the k^{th} DDE, called the nodal point, is therefore located at the x position

$$x_k = -L + \sum_{j=1}^{k} h_j - a_1.$$

Although curved cracks with shapes more general than a straight line may be discretely approximated using the DDM [8], the line crack problem will be sufficient to illustrate the method. Also, since the line crack problem has been solved analytically, the quality of the DDM numerical solution will be evident.

The stress relations for a single DDE, (3.9)-(3.11), in conjunction with the crack boundary conditions, allow the construction of a linear system of equations which may be solved for the resulting DD amplitudes. Specifically, the no shear stress BC at the DDE midpoints,

$$\sigma_{xy}(x_k, 0) = 0, \qquad k = 1, .., N,$$

along with (3.11) implies that

$$D_x^k = 0, \qquad k = 1, .., N.$$

The normal stress BC applied at the DDE midpoints,

$$\sigma_{yy}(x_k, 0) = -p(x_k), \qquad k = 1, ..., N,$$

along with the linear superposition of the resultant DDE stresses,

$$\sigma_{yy}(x_k, 0) = \sum_{j=1}^{N} \sigma_{yy}^{j}(x_k, 0), \qquad k = 1, ..., N,$$

and (3.10) yield the condition

$$-p(x_k) = \sum_{j=1}^{N} \sigma_{yy}^{j}(x_k, 0), \qquad k = 1, ..., N,$$

where

$$\sigma_{yy}^{j}(x_k, 0) = -\frac{G}{\pi(1-\nu)} \frac{a_j}{(x_j - x_k)^2 - a_j^2} D_y^j, \qquad j = 1, ..., N,$$

is the normal stress at $x = x_k$ resulting from the j^{th} DDE. The resulting matrix equation to be solved for the unknown DDE normal displacements, $\{D_y^j\}_{j=1}^N$, is

$$-p_k = \sum_{j=1}^{N} A_{kj} D_y^j, \qquad k = 1, ..., N, \tag{3.12}$$

where $p_k = p(x_k)$ and

$$A_{kj} = -\frac{G}{\pi(1-\nu)} \frac{a_j}{(x_j - x_k)^2 - a_j^2}, \qquad k, j = 1, ..., N, \tag{3.13}$$

are called the DDE influence coefficients. The resulting DDE amplitudes, D_y^j, may be interpreted as the (negative) width of the crack at the midpoint of the j^{th} element located at the nodal points, x_j. This method is also called a PWC collocation method since stress is collocated at the nodes of the DDE.

For the symmetric problem where

$$p(x) = p(-x),$$

the resulting displacement solution is also symmetric:

$$D_y^j = D_y^{N+1-j}, \qquad j = 1, ..., N.$$

In this case, it is unnecessary to solve the dense N-by-N system of equations (3.12) when an $\frac{N}{2}$-by-$\frac{N}{2}$ system (for N even) will produce an equivalent result. A formula for constructing the $\frac{N}{2}$-by-$\frac{N}{2}$ influence matrix from A_{kj}, for the positive x-axis, is given in Appendix B.

Calculation of Stress Intensity Factors

Since stress intensity factors play such a central role in characterizing fractures in LEFM, it is necessary to be able to numerically approximate them with sufficient accuracy. A direct approach that is commonly used is to use the asymptotic form of the normal displacement, $u_y(x, 0_+)$, at the crack tip. Using (2.5) the asymptotic relation is

$$u_y(x, 0_+) \overset{x \to L}{\sim} \frac{4K_I}{E'} \sqrt{\frac{L-x}{2\pi}}. \tag{3.14}$$

The stress intensity factor is then approximated as

$$K_I \approx \frac{E'}{8} \sqrt{\frac{2\pi}{L-x_*}} U_y^*, \tag{3.15}$$

where $U_y^* \approx 2u_y(x, 0_+)$ is the width of the crack at a distance $L - x_* \ll L$ from the crack tip. Typically U_y^* is the magnitude of the DDE closest to the tip. In order to be effective, this approach clearly requires high resolution at the crack tip. Higher accuracy crack tip elements, and/or relatively more dense distributions of DDE near the tip are often used to improve the accuracy of the crack tip solution. For example, in addition to a special squareroot displacement crack tip element, Raveendra and Cruse [25] have used constant elements of width h, except for near the tip where four individual DDE of width $\frac{h}{4}$ were used.

An alternate approach for estimating K_I is to use equation (2.29). Since the strain energy, per unit thickness, of a half-crack of length L is

$$W_0(L) = \int_0^L p(x) u_y(x) dx, \tag{3.16}$$

a simple numerical approximation, using constant DDE of width h_k, is

$$\hat{W}_0(L) \doteq -\frac{1}{2}\sum_{k=1}^{N} p(x_k) D_y^k h_k.$$

Then, using a difference approximation such as

$$\frac{\partial W_0(L)}{\partial L} = \frac{\hat{W}_0(L+h) - \hat{W}_0(L-h)}{2h} + O(h^2), \tag{3.17}$$

the stress intensity factor may calculated from (2.29) using

$$K_I = \sqrt{E' \frac{\partial W_0(L)}{\partial L}}. \tag{3.18}$$

In cases where higher accuracy is required and/or more sophisticated DDMs are used, a more appropriate approximation of (3.16) and its derivative should be used.

Examples of the asymptotic and the strain energy release rate methods for calculating K_I are presented in Chapter 5.

Crack Tip Elements

A simple way to improve the accuracy of the DDM crack solution is to combine the constant DDE with special crack tip elements. These tip DDE incorporate the known asymptotic dependence of the displacement solution in the neighbourhood of the tip (see (2.3)) in order to calculate more accurate influence coefficients for stress BVPs. In general, for a mixed BVP (i.e., a BVP where a mixture of normal and shear component stresses and displacements are specified on the boundary), asymptotic crack tip elements may be used for both the stress and displacement fields. For example, Raveenda and Cruse [25] consider displacement, $u(r)$, and traction, $t(r)$, tip parametrizations of the form

$$\begin{aligned} u(r) &= U_1 + U_2\sqrt{\frac{r}{l}} + U_3\frac{r}{l} \\ t(r) &= T_1\sqrt{\frac{l}{r}} + T_2 + T_3\sqrt{\frac{r}{l}}. \end{aligned}$$

where $\{U_j\}_{j=1}^3$, $\{T_j\}_{j=1}^3$ are expressed in terms of the nodal element amplitudes, e.g., DDE amplitudes and the traction element amplitudes. However, in the following, only stress BVPs will be considered.

Calculation of the normal stress along the x-axis resulting from a general DDE shape,

$$\hat{u}_y(x) = u_x(x, 0_-) - u_x(x, 0_+) < 0, \tag{3.19}$$

when $x \in [x_1, x_2]$, will use the fact that

$$\sigma_{yy}(x, 0) = \frac{-G}{2\pi(1-\nu)} \lim_{y \to 0} \int_{x_1}^{x_2} \frac{\hat{u}_y(\xi)}{(x-\xi)^2 + y^2} d\xi \tag{3.20}$$

for $x \neq x_1, x_2$ [8].

It is easy to verify that $\sigma_{yy}(x, 0)$, as given by (3.10), results from (3.20) when

$$\hat{u}_y(x) = \begin{cases} D_y, & x \in (-a, a), \\ 0, & \text{otherwise.} \end{cases}$$

"Squareroot Displacement" Crack Tip Element

Since the asymptotic crack tip width depends on the square-root of the distance from the tip (see (3.14)), consider a tip element of length $h = 2a$ and (-ve) width given by

$$\hat{u}_y(x) = u_x(x, 0_-) - u_x(x, 0_+) = \begin{cases} D_y \sqrt{\frac{x}{a}}, & x \in (0, 2a), \\ 0, & \text{otherwise.} \end{cases} \tag{3.21}$$

Note that the crack is located in the $x > 0$ region. Evaluation of (3.20) yields

$$\sigma_{yy}(x, 0) = \frac{-G}{2\pi(1-\nu)} \begin{cases} \frac{\sqrt{2}}{x-2a} + \frac{1}{2\sqrt{ax}} \ln \left| \frac{\sqrt{x}-\sqrt{2a}}{\sqrt{x}+\sqrt{2a}} \right|, & x > 0, \\ \frac{1}{\sqrt{a(-x)}} \left[\arctan \sqrt{\frac{2a}{(-x)}} - \frac{\sqrt{2a(-x)}}{2a-x} \right] & x < 0. \end{cases} \tag{3.22}$$

The same argument used to derive (3.13) leads to the use of

$$A_{kj} = \frac{-G}{2\pi(1-\nu)}\left[\frac{\sqrt{2}}{X_{kj}-2a_j} + \frac{1}{2\sqrt{a_j X_{kj}}}\ln\left|\frac{\sqrt{X_{kj}}-\sqrt{2a_j}}{\sqrt{X_{kj}}+\sqrt{2a_j}}\right|\right], \qquad j = 1 \text{ or } N$$

where $X_{kj} = a_j + |x_k - x_j|$. Hence, the tip element amounts to changing the influence coefficients for $2N$ elements of the influence matrix, A_{kj}. Also, the long distance character of the tip element influence coefficient is different from that of the constant tip element, since

$$A_{kj} \sim \frac{-G}{\sqrt{2}\pi(1-\nu)}\frac{1}{|x_k - x_j|}, \qquad |x_k - x_j| \gg a_j,$$

while the constant tip has the inverse square distance dependence (see (3.13)).

While the squareroot tip element does reduce overall crack error and improves the tip accuracy, there is a limit to the increase in accuracy that a single DDE tip correction can provide. Also, since the squareroot tip correction only involves one element, the relative importance of the crack tip element becomes negligible as N gets larger. One disadvantage of the crack tip element is that O(N) influence coefficients must be modified.

Piecewise Linear Collocation and Higher-order DDMs

The use of higher-order DDE with more degrees of freedom than the constant DDE is a natural choice for achieving a more accurate approximation of the crack width. However, higher-order DDMs are more difficult to formulate and implement, especially in higher dimensions. Also, the resulting linear system of equations has different properties which can make it more difficult to solve approximately in the case when N is very large. Nevertheless, higher-order methods can be relied upon to yield significantly more accurate results than the ordinary PWC DDM. In the following, the case of linear elements will be considered. The PWL DDM will be referred to as the piecewise linear collocation (PWLC) method.

Consider a PWL DDE of length $h = 2a$ and lying along the x-axis from $x = -a$ to $x = a$. Assume, for simplicity, that the shear discontinuity component is zero and that the normal discontinuity is given by $D_N(x)$, $x \in (-a, a)$. While (2.16) could be used to calculate the stress at points along the x-axis resulting from an arbitrary DDE, Crawford and Curran [5] have given expressions for the stresses and displacements associated with a general two-dimensional DDE (see Appendix A.). Using the expression for σ_{yy}, the stress along the x-axis is

$$\sigma_{yy}(x,0) = \frac{G}{2\pi(1-\nu)} \lim_{y\to 0} \left(\frac{\partial}{\partial y} - y\frac{\partial^2}{\partial y^2} \right) \int_{-a}^{a} \frac{y}{(x-\varepsilon)^2 + y^2} D_N(\varepsilon) d\varepsilon. \tag{3.23}$$

By choosing to collocate stresses along the PWL element at nodal positions given by the Gauss-Chebyshev integration points, good convergence properties are obtained [5]. Accordingly, the linear DDE is written as

$$D_N(x) = N_1(x)D_1 + N_2(x)D_2 \tag{3.24}$$

where D_1, D_2 are the nodal displacements and

$$\begin{aligned} N_1(x) &= \frac{1}{\sqrt{2}} \left(\frac{1}{\sqrt{2}} - \frac{x}{a} \right) \\ N_2(x) &= \frac{1}{\sqrt{2}} \left(\frac{1}{\sqrt{2}} + \frac{x}{a} \right). \end{aligned}$$

Substitution of (3.24) into (3.23) yields

$$\sigma_{yy}(x,0) = \frac{G}{2\pi(1-\nu)} \left[F(x,-1)D_1 + F(x,+1)D_2 \right] \tag{3.25}$$

where

$$F(x,n) = \frac{a}{x^2 - a^2} + n\sqrt{2} \left[\frac{x}{x^2 - a^2} + \frac{1}{2a} \ln \left| \frac{x-a}{x+a} \right| \right]. \tag{3.26}$$

This result can then be used to construct an approximate solution of the pressurized line crack problem. The construction of the PWLC matrix equation is detailed in Appendix C.

An easy way to increase the accuracy of the PWLC method is to use a crack tip element, such as (3.21), at each end of the crack. The stress influence of the tip element is given by (3.22). For purposes of numerical comparison, a tip element of the same length as the linear element will be used. The tip element significantly reduces the error at the crack tip, as will be shown in Chapter 5.

Self-effect Tip Corrections for Piecewise Constant DDE

Based on the success of the crack tip element, it is clear that numerical accuracy at the fracture tip plays an important role in the overall accuracy of the solution. The strong dependence of crack width accuracy on crack tip influence coefficients is reasonable since the influence matrix is an approximation of a Fredholm integral operator which is singular at the crack tips. In fact, it will be illustrated that large changes in the accuracy of the crack width solution can be achieved by simply correcting the tip influence coefficients. In the most extreme case, only a single number in the influence matrix, the crack tip self-effect, is changed. The correction may be interpreted as introducing corrective stresses at the tip (or edge) elements which reduce the crack width overestimation characteristic of the PWC DDM [27].

Modelling a crack which has a length that is not a multiple of the constant grid of size h is also considered. This is often refered to as a fractionally mined crack.

The Quarter-grid Correction Scheme

Using the "method of rational functions," Ryder and Napier [27] were able to analytically study the error associated with DDM modelling of cracklike tabular stress problems on a uniform grid. Error analysis of the piecewise constant DDM solution of a pressurized line crack, for constant pressure, on a constant grid of size h indicated a quarter grid discretization error in the crack width. Using this insight,

a correction strategy was created which multiplied the self-effect influence coefficients corresponding to the crack tip elements by a factor. This edge/tip correction also supported nondiscrete positioning of the mining edges, i.e., fractional mining. Therefore, by simply correcting the edge self-effects, the numerical method could more accurately coincide with the location of the excavation edges. This is convenient since perfect alignment of the excavation with the grid is often inconvenient. In addition to 2D crack problems, the approach was also found to be enhance the numerical modelling of 3D excavations (see [27], [21]).

The complete definition of this correction process was given by Ryder and Napier [27] as follows:

> Prior to preparing problem input in the form of fixed-size grids, conceptually reduce the area mined by moving all faces inward by $\frac{1}{4}$-grid. Let m be the resulting edge grid fraction mined $(0 < m \leq 1)$. Numerically increase the normalized edge self-effects by $\alpha = (1-m)/m$.

For example, for a nonfractionally mined grid with DDE of length h, reducing the edge elements by $\frac{h}{4}$ implies that $m = \frac{3}{4}$. Therefore,

$$\alpha = \frac{1 - \frac{3}{4}}{\frac{3}{4}} = \frac{1}{3}$$

and the edge effects must be multiplied by

$$\omega = 1 + \alpha = \frac{4}{3},$$

i.e., increased by approximately 33%.

In general, let the grid be of length h and the crack tip element of length λh. In this case $m = \frac{3}{4}\lambda$ and since $m \in (0, 1]$ therefore $\lambda \in (0, \frac{4}{3}]$. The self-effect formula gives

$$\alpha_{\text{quarter-grid}}(\lambda) = \frac{1-m}{m} = \frac{4}{3\lambda} - 1 \tag{3.27}$$

so that the self-effect multiplier is

$$\omega_{\text{quarter-grid}} = 1 + \alpha_{\text{quarter-grid}} = \frac{4}{3\lambda}.$$

Numerically Determined Crack Tip Self-effect Correction Schemes

The quarter-grid correction scheme was analytically derived in order to provide a reduction in crack width error in the case of a constant pressure distribution. In order to find other error reducing tip element self-effect correction schemes a numerical approach was considered. The approach used involves solving for the required self-effect tip correction subject to the minimization of a relevant error. Symmetric pressure distributions with $p(x) \geq 0$ were considered which guarantees that the stress intensity factor is nonzero (see (2.19)) and that a squareroot crack tip of the form (3.14) exists.

Far-field Collocation Correction Strategy

In this case, the error of the DDE closest to $x = 0$ is minimized. In particular, discretize the crack using $2N$ constant DDE each of length $h = 2a = \frac{N}{L}$. Let $\omega = (1+\alpha)$ be the self-effect multiplier. Use the parametrized $2N \times 2N$ influence matrix, $A(\alpha)$, to construct the $N \times N$ influence matrix, $B(\alpha)$, for the positive interval $x \in (0, L)$ (see (B.6)). Then solve (B.5) to find $\hat{D}_y^k$, $k = 1, ..., N$. Use

$$E_{\text{middle}} = \left| \left| \hat{D}_y^1 \right| - 2u_y(h) \right|$$

as a measure of the error of the solution near the middle of the crack, where u_y is the height of the upper crack face given by (2.8). In this fashion, for a given N, find $\alpha = \alpha_N$ such that $E_{\text{middle}} = 0$. Since collocation of the solution near the middle of the crack (far from the stress singularity) is used to determine the required stress self-effect correction at the crack tip, this approach has been called the "far-field"

	N					
	5	10	20	40	100	500
p_0	0.2635	0.2636	0.2623	0.2621	0.2620	0.2620
$p_0(1-\frac{x}{L})$	0.2346	0.2476	0.2546	0.2581	0.2603	0.2620

Table 3.1: Alpha values for the far-field correction.

correction scheme. Numerically determined α corrections are shown in Table 3.1 for constant and linearly decreasing pressure distributions. Based on these results, the far-field correction strategy is to choose

$$\alpha_{\text{far-field}} = 0.26$$

and therefore increase the tip element self-effect by 26%.

Tip Collocation Correction Strategy

The tip collocation correction is constructed like the far-field collocation correction, with the exception that the error minimized is that of the DDE closest to the tip. Numerically determined α corrections for the tip collocation method are shown in Table 3.2 for constant and linearly decreasing pressure distributions. Based on these results, the tip collocation strategy is to choose

$$\alpha_{\text{tip-collocation}} = 0.20 \tag{3.28}$$

and therefore increase the tip element self-effect by 20%.

A Scaled Quarter-grid Correction

Unlike the quarter-grid correction, the numerically determined collocation corrections do not include the fractional mining parameter λ. However, it was found that the collocation corrections provided better accuracy than the quarter-grid cor-

	N					
	5	10	20	40	100	500
p_0	0.2065	0.2027	0.2008	0.1999	0.1993	0.1990
$p_0(1-\frac{\pi}{L})$	0.1801	0.1889	0.1938	0.1963	0.1979	0.1987

Table 3.2: Alpha values for the tip collocation correction.

rection in the case $\lambda = 1$. In an attempt to construct a collocation self-effect correction that included λ dependence, the following scaled quarter-grid-like corrections were constructed:

$$\begin{aligned} \alpha_{\text{far-field}}(\lambda) &= \frac{\alpha_{\text{quarter-grid}}(\lambda)}{\alpha_{\text{quarter-grid}}(0)}\alpha_{\text{far-field}} \\ \alpha_{\text{tip-collocation}}(\lambda) &= \frac{\alpha_{\text{quarter-grid}}(\lambda)}{\alpha_{\text{quarter-grid}}(0)}\alpha_{\text{tip-collocation}} \end{aligned} \tag{3.29}$$

A Fractionally Mined Crack Tip Element

Consider the case of a crack which has a length that is not a multiple of a constant grid of size h. This is refered to as a fractionally mined crack. Having a technique, such as the quarter-grid correction scheme, that allows the accurate modelling of a fractionally mined crack on a constant grid is very useful. In addition, the fact that the quarter-grid scheme only requires the modification of the single crack tip self-effect influence coefficient allows the method to be generalized to problems of higher dimensions. It would therefore be useful to develop other correction strategies that allow fractional mining yet only require the modification of local crack tip influence coefficients. Since crack tip self-effect correction strategies were considered in the previous section, now consider constructing a crack tip influence correction for the neighbouring element. The strategy used will be to construct a tip element that includes an extension element for the fractionally

mined crack part. The extension element will produce an extra contribution to the ordinary constant DDE. By limiting the influence of the extra contribution to the tip and neighbouring elements, a local correction is achieved. Finally, a self-effect correction on the tip element, similar to the tip collocation scheme, leads to improved accuracy.

Consider a piecewise constant tip element of length $\lambda h = 2\lambda a$ for $1 \leq \lambda \leq 2$. The "main" part of the element will be of width $-D_y$ and length $h = 2a$. The "extension" part of the element is of length $(\lambda - 1)h$ and lies between the main element and the actual crack tip. The width of the extension element is to be determined by the asymptotic requirement that the DDE width at the midpoints of the main and extension elements is consistent with the scaling

$$|D| \propto \sqrt{x}, \qquad \text{as } x \to 0. \tag{3.30}$$

Specifically, the piecewise constant DDE width is chosen as

$$\hat{u}_y(x) = u_x(x, 0_-) - u_x(x, 0_+) = \begin{cases} \Delta D_y, & x \in (0, (\lambda - 1)h), \\ D_y, & x \in ((\lambda - 1)h, \lambda h) \\ 0, & \text{otherwise,} \end{cases}$$

where

$$\Delta = \sqrt{\frac{\lambda - 1}{2\lambda - 1}}. \tag{3.31}$$

The main crack opening is therefore located in the $x > \lambda h$ region.

Since the variable length tip element consists of two piecewise constant DDE, the resulting induced normal stress may be calculated as the sum of two stress contributions, individually given by (3.10). Denoting the midpoint of the main element by $x_m = (\lambda - \frac{1}{2})h$, the midpoint of the extension element by $x_e = \frac{\lambda - 1}{2}h$ and the length of the extension element by $h_e = 2a_e$, the normal stress resulting from

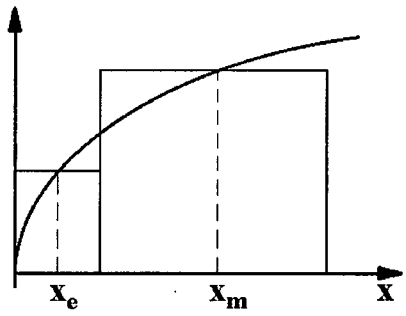

Figure 3.1: The fractional mining tip.

the crack tip is

$$\begin{aligned}
\sigma_{yy}(x,0) &= \text{(stress from "main" element)} + \\
&\quad \text{(stress from "extension" element)} \\
&= \left(\frac{-G}{\pi(1-\nu)}\frac{a}{(x-x_m)^2-a^2}D_y\right) + \left(\frac{-G}{\pi(1-\nu)}\frac{a_e}{(x-x_e)^2-a_e^2}\Delta D_y\right) \\
&= \frac{-G}{\pi(1-\nu)}\left\{\frac{a}{(x-x_m)^2-a^2} + \frac{a_e}{(x-x_e)^2-a_e^2}\Delta\right\} D_y
\end{aligned}$$

Using this result, the influence coefficients for the crack tip are readily obtainable for a particular nodal discretization, $x = x_k$, $k = 1, ..., N$.

A local tip element is then achieved by only allowing the extension element to influence the tip element and the neighbouring element. The self-effect correction strategy used only modifies the self-effect of the main element. The main element's self-effect is multiplied by

$$\begin{aligned}
\omega &= 1 + \alpha(\lambda) \qquad (3.32) \\
&= 1 + \frac{\alpha_{\text{tip-collocation}}}{\lambda}.
\end{aligned}$$

Numerical experiments suggested that when the extension element's corrective stresses were limited to the main element and the neighbouring element, that modification of the stress influence of the neighbouring element on the tip would also

aid the correction. The additional corrective stress that that was chosen for the one neighbouring DDE applied to the crack tip was

$$\frac{-G}{\pi(1-\nu)}\frac{a}{(x-x_e)^2-a^2}\Delta\,.$$

While this strategy is ad hoc, it is consistent with the tip collocation method when $\lambda = 1$ and good numerical solutions are obtained for $\lambda \in [1,2]$. Also, since the tip correction scheme affects only the nearest neighbours, the method is consistent with the constant DDM in the limit that $N \to \infty$.

Chapter 4

A Galerkin Finite Element Method

The Galerkin approach is to represent the crack width as the sum of basis functions with compact support and then to use (2.16), or the equivalent equation on $(-L, L)$, to construct a discrete relation between crack width and pressure. An approximate weak solution of (2.15) may then be constructed by taking the inner product of both sides with suitable test functions, $v(x)$, and then integrating by parts. Specifically, start from (2.15),

$$p(x') = -\frac{E'}{\pi}\int_0^L \frac{du_y(x)}{dx}\frac{x}{x^2 - x'^2}dx,$$

which is equivalent to (2.16), then take the inner product with $v(x')$

$$\begin{aligned}\int_0^L p(x')v(x')dx' &= -\frac{E'}{\pi}\int_0^L dx'\int_0^L dx\frac{du_y(x)}{dx}\frac{x}{x^2 - x'^2}v(x') \\ &= \frac{E'}{\pi}\int_0^L dx\frac{du_y(x)}{dx}x\int_0^L dx'\frac{v(x')}{x'^2 - x^2}. \end{aligned} \tag{4.1}$$

Using the fact that

$$\int \frac{dx'}{x'^2 - x^2} = -\frac{1}{2x}\ln\left|\frac{x + x'}{x - x'}\right| + \text{constant},$$

(4.1) can be integrated by parts:

$$\begin{aligned}\int_0^L p(x')v(x')dx' &= \frac{E'}{\pi}\int_0^L dx\frac{du_y(x)}{dx}x\int_0^L dx'\frac{v(x')}{x'^2 - x^2} \\ &= \frac{E'}{\pi}\int_0^L dx\frac{du_y(x)}{dx}x\left\{-\frac{1}{2x}\ln\left|\frac{x + x'}{x - x'}\right|v(x')\right|_{x'=0}^{x'=L}\end{aligned}$$

$$-\int_0^L dx' \left(-\frac{1}{2x}\ln\left|\frac{x+x'}{x-x'}\right|\right)\frac{dv(x')}{dx'}\Bigg\}$$

$$= \frac{E'}{2\pi}\int_0^L dx \int_0^L dx' \ln\left|\frac{x+x'}{x-x'}\right| \frac{dv(x')}{dx'}\frac{du_y(x)}{dx}, \tag{4.2}$$

where the condition that $v(L) = 0$ was required. Finally, written in terms of the full crack width, $w(x) = 2u_y(x)$, equation (4.2) becomes

$$\int_0^L p(x')v(x')dx' = \frac{E'}{4\pi}\int_0^L dx \int_0^L dx' \ln\left|\frac{x+x'}{x-x'}\right| \frac{dv(x')}{dx'}\frac{dw(x)}{dx}. \tag{4.3}$$

Note that while this representation is in terms of crack width derivatives, a non-derivative formulation can also be constructed using (2.16). However, (4.3) is convenient for use with the piecewise linear basis functions given in the following section.

Piecewise Linear (PWL) Basis Functions

Assume that the interval $(0, L)$ has been partitioned by the points $\{x_k\}_{k=0}^{N+1}$, where

$$0 = x_0 = x_1 < x_2 < \cdots < x_{N-1} < x_N < x_{N+1} = L$$

Let $\Lambda_k = \{x | x \in (x_k, x_{k+1})\}$, $k = 0, 1, ..., N$. Note that $x_0 = 0$ and $\Lambda_0 = \{\emptyset\}$ have been introduced for notational convenience. The set of piecewise linear basis functions will be $\{\phi_k(x)\}_{k=1}^{N}$ for $x \in (0, L)$. These functions will be consistent with the crack width boundary condition

$$u_y(L) = 0.$$

A suitable choice of basis functions are the hat-like functions

$$\phi_k(x) = \begin{cases} m_{k-1}(x - x_{k-1}), & x \in \Lambda_{k-1}, \\ m_k(x_{k+1} - x), & x \in \Lambda_k, \\ 0, & \text{otherwise}, \end{cases} \quad , \quad k = 1, 2, ..., N, \tag{4.4}$$

where

$$m_k = \begin{cases} 0, & k = 0, \\ (x_{k+1} - x_k)^{-1}, & k = 1, ..., N. \end{cases} \tag{4.5}$$

Notice that $\phi(x_k) = 1$, $k = 1, ..., N$. Accordingly, the crack solution will be approximated at $\{x_k\}_{k=1}^N$.

PWL Basis Functions with a Crack-tip Correction

From the DDM, it is known that incorporating the square root dependence of the width near the crack tip (see (2.5)) can lead to a significant improvement in the accuracy of the width solution. The Galerkin approach also benefits from the use of a special square root tip element near the crack tip. Let $\left\{\hat{\phi}_k(x)\right\}_{k=1}^N$ be the new basis that incorporates the special tip. Specifically, define

$$\hat{\phi}_k(x) = \phi_k(x), \qquad k = 1, ..., N-1, \tag{4.6}$$

and

$$\hat{\phi}_N(x) = \begin{cases} m_{N-1}(x - x_{N-1}), & x \in \Lambda_{N-1}, \\ m_N\sqrt{(L-x)(L-x_N)}, & x \in \Lambda_N, \\ 0, & \text{otherwise} \end{cases} \tag{4.7}$$

Matrix Equations

Using the basis functions $\{\phi_k(x)\}_{k=1}^N$ $\left(\text{or } \left\{\hat{\phi}_k(x)\right\}_{k=1}^N\right)$ it is possible to approximate the crack width $w(x)$ by the sum

$$w(x) \approx \sum_{n=1}^{N} W_n \phi_n(x).$$

Then, by letting $v(x) = \phi_n(x)$, $n = 1, 2, ..., N$, (4.3) yields the system of equations

$$\int_0^L p(x)\phi_n(x)dx = \sum_{m=1}^{N}\left[\frac{E'}{4\pi}\int_0^L dx' \int_0^L dx \ln\left|\frac{x+x'}{x-x'}\right| \frac{d\phi_n(x')}{dx'}\frac{d\phi_m(x)}{dx}\right] W_m, \qquad n = 1, 2, ..., N. \tag{4.8}$$

By making the approximation

$$\int_0^L p(x)\phi_n(x)dx \approx P_n \int_0^L \phi_n(x)dx,$$

with $P_n = p(x_n)$, then (4.8) becomes the linear system of equations

$$MP = SW, \tag{4.9}$$

where M is the $N \times N$ diagonal weight matrix,

$$M_{nm} = \delta_{nm} \int_0^L \phi_n(x)dx, \tag{4.10}$$

S is the $N \times N$ stress influence matrix,

$$S_{nm} = \frac{E'}{4\pi} \int_0^L dx' \int_0^L dx \ln \left| \frac{x+x'}{x-x'} \right| \frac{d\phi_n(x')}{dx'} \frac{d\phi_m(x)}{dx}, \tag{4.11}$$

and

$$\begin{aligned} P &= (P_1, P_2, \cdots, P_N)^T, \\ W &= (W_1, W_2, \cdots, W_N)^T. \end{aligned}$$

If the square root tip corrected basis functions are used, all $\phi(x)$ functions are replaced by $\hat{\phi}(x)$. The weight and stress matrices are calculated in Appendix D.. Numerical results are presented in the next chapter.

Strain Energy Calculation Method

When calculating the strain energy of a half-crack, a direct approach is to approximate (3.16). For example, this is done in the next chapter when estimating stress intensity factors using the strain energy release rate method (see p.42). The integral has been estimated as

$$\begin{aligned} \int_0^L p(x)w(x)dx &\approx \int_0^L p(x) \left(\sum_{k=1}^N W_k \phi_k(x) \right) dx \\ &\approx \sum_{k=1}^N p(x_k) W_k \int_0^L \phi_k(x)dx \\ &= \sum_{k=1}^N p(x_k) W_k M_{kk} \end{aligned}$$

where the definition of the weighting matrix (4.10) has been used. On a constant grid, this is consistent with the midpoint rule, except for the endpoints which are slightly different. When the tip-corrected basis functions are used, the weighting matrix changes accordingly.

Chapter 5

Comparison of Numerical Methods

This chapter presents numerical results for the various crack width methods.

Relative Error Notation

The relative error of a width w_k at nodal position x_k is defined to be

$$E_k = \frac{w_k - w_{\mathbf{exact}}(x_k)}{w_{\mathbf{exact}}(x_k)}, \qquad k = 1, 2, ..., N_{\max},$$

where $N_{\max}$ is the number of nodes for the method. The error at the crack tip will be calculated using

$$E_{tip} = E_{N_{\max}}.$$

The error near the middle of the crack will be estimated using

$$E_{mid} = E_1.$$

An average error is calculated using

$$\bar{E} = \frac{1}{N_{\max}} \sum_{n=1}^{N_{\max}} |E_k| .$$

The fact fact that the width methods have differing nodal numbers, $N_{\max}$, and positions should be kept in mind when comparing errors.

Shortened Name	Description
PWCC	piecewise constant collocation DDM (ordinary DDE)
PWCC-tip	PWCC with squareroot tip element (tip length = ordinary DDE length)
PWCC-QGrid	PWCC with quarter-grid self-effect correction ($\alpha = \frac{1}{3}$)
PWCC-far-field	PWCC with far-field self-effect correction ($\alpha = 0.26$)
PWCC-tip-coll	PWCC with tip collocation self-effect correction ($\alpha = 0.20$)
Galerkin	Galerkin with $\{\phi_k\}_{k=1}^N$ basis functions
Galerkin-tip	Galerkin with $\{\hat{\phi}_k\}_{k=1}^N$ basis functions
PWLC	piecewise linear collocation DDM (linear DDE)
PWLC-tip	PWLC with squareroot tip element (tip length = linear element length)

Table 5.1: Naming conventions adopted for crack width methods.

Crack Width Results

This section presents the results of the crack width methods for comparison. For convenience a shortened name has been assigned to each of the methods and is shown in Table 5.1.

It is important to compare the methods fairly with respect to computational effort. This means that methods will be compared based on the number of nodes (degrees of freedom) that are used and not the number of elements. Let N be the number of nodes on the interval $[0, L)$, with the exception of the PWLC-tip method which has $N - 1$ nodes.

The methods are demonstrated for the constant pressure case. The accuracy trends that exist for this case tend to also continue for other pressure distributions that have $p(x) \geq 0$, and therefore a nonzero stress intensity factor. For the sake of brevity only the constant pressure results are presented.

The results of the ordinary element based methods (PWCC, PWCC-tip, PWCC-

	E_{mid} (% or units of 0.01)				
	N				
	4	10	20	40	100
PWCC	+6.54	+2.54	+1.26	+0.627	+0.250
PWCC-tip	+4.55	+1.61	+0.778	+0.382	+0.151
PWCC-QGrid	-1.20	-0.476	-0.239	-0.120	-0.0479
PWCC-far-field	+0.0686	+0.0201	+0.00835	+0.00371	+0.00137
PWCC-tip-coll	+1.25	+0.482	+0.238	+0.118	+0.0471
Galerkin	-2.29	-1.05	-0.551	-0.282	-0.114
Galerkin-tip	+0.548	+0.0810	+0.0188	+0.00406	+0.000357
PWLC	-1.32	-0.837	-0.519	-0.306	-0.146
PWLC-tip	+5.00	-0.109	-0.385	-0.291	-0.151

Table 5.2: Mid-crack relative error for width calculation methods.

QGrid, PWCC-far-field, PWCC-tip-coll) are plotted in Fig. 5.1 for $N = 10$ and Fig. 5.2 for $N = 20$. The low tip error of the PWCC-tip-coll method and the low mid-crack error of the PWCC-far-field method are clearly apparent. The higher-order PWL methods (Galerkin, Galerkin-tip, PWLC, PWLC-tip) are demonstrated in Fig. 5.3 for $N = 10$ and Fig. for $N = 20$. The three relative errors, E_{mid}, E_{tip} and $\bar{E}$, are shown in tables 5.2, 5.3 and 5.4, respectively. Note that part of the reason the PWLC method has such a large relative error at its tip node is because the tip node is closer to $x = L$ than the tip nodes of any of the other methods.

Quarter-grid Methods and Fractional Mining

The quarter-grid method has already been demonstrated, for the case $\lambda = 1$, in Fig. 5.1 and Fig. 5.2, where it was compared to the other PWCC related

	E_{tip} (in % or units of 0.01)				
	N				
	4	10	20	40	100
PWCC	+27.4	+26.1	+25.7	+25.5	+25.4
PWCC-tip	+9.55	+8.59	+8.31	+8.17	+8.08
PWCC-QGrid	-11.4	-11.8	-11.9	-12.0	-12.0
PWCC-far-field	-5.06	-5.54	-5.69	-5.76	-5.81
PWCC-tip-coll	+0.878	+0.732	+0.0813	-0.0130	-0.0989
Galerkin	+3.25	+2.25	+2.22	+2.21	+2.20
Galerkin-tip	+2.84	+1.08	+0.782	+0.639	+0.555
PWLC	+11.7	+11.9	+11.9	+12.0	+12.1
PWLC-tip	+6.91	+1.08	+0.782	+0.639	+0.555

Table 5.3: Crack tip relative error for width calculation methods.

	$\bar{E}$ (in % or units of 0.01)				
	N				
	4	10	20	40	100
PWCC	+13.0	+6.32	+3.59	+2.01	+0.917
PWCC-tip	+7.04	+3.47	+1.98	+1.12	+0.515
PWCC-QGrid	+4.10	+1.95	+1.08	+0.586	+0.258
PWCC-far-field	+1.34	+0.609	+0.318	+0.163	+0.0665
PWCC-tip-coll	+1.33	+0.678	+0.407	+0.241	+0.118
Galerkin	+2.87	+1.53	+0.962	+0.581	+0.286
Galerkin-tip	+1.29	+0.293	+0.122	+0.0541	+0.0196
PWLC	+3.91	+2.00	+1.19	+0.702	+0.345
PWLC-tip	+6.53	+0.510	+0.387	+0.348	+0.232

Table 5.4: Average relative error for width calculation methods.

methods. It can be seen that, while the PWCC-QGrid result is clearly better than the PWCC result, it still has around 12% relative error at the crack tip. However, the scaled quater-grid methods, which use (3.29), do not have this property since they are identical to the PWCC-far-field and PWCC-tip-coll methods when $\lambda = 1$. Numerical results for the three quarter-grid related methods are shown in Fig. 5.5 for λ =0.8, 1, 1.2. It should be noted that the quarter-grid correction was designed for $\lambda \in (0, \frac{4}{3}]$. While the two scaled quarter-grid methods are both very accurate for $\lambda = 1$ and do not produce such large tip errors as the PWCC-QGrid method, it becomes clear for different λ that the corrections do not eradicate the error. It should be noted that, although the errors are significant for all three methods, they are still comparable to the error of the PWCC method. Based on the evidence it may be mildly favourable to use the 0.26 scaled quarter-grid method instead of just quarter-grid.

Fractional Mining Tip Correction

Some numerical results for the fractional mining tip correction (see p. 28) are presented in Fig. 5.6 for λ=1.0, 1.2, 1.5, 2.0 for $N = 10$. Results for the quarter-grid method are also included for λ=1.0 and 1.2. Small crack tip error for various λ is a feature of the fractional mining tip that is not shared by the quarter-grid-like corrections. Although the overall error is getting worse as λ approaches 2, the solution is still reasonably accurate. However, a notable point is that good tip error results are obtained for all the λ values in the figure.

Stress Intensity Factor Estimation

This section provides stress intensity factors calculated using various numerical crack width methods. The stress intensity factors are estimated using both the

	Stress Intensity Factor (units of $p_0\sqrt{\pi L}$)				
	N				
	4	10	20	40	100
PWCC	1.2339	1.2455	1.2494	1.2514	1.2525
PWCC-tip	1.0607	1.0722	1.0763	1.0783	1.0795
PWCC-QGrid	0.8576	0.8711	0.8755	0.8777	0.8790
PWCC-far-field	0.9193	0.9327	0.9372	0.9394	0.9407
PWCC-tip-coll	0.9767	0.9901	0.9945	0.9967	0.9981
Galerkin	0.9577	0.9966	1.0093	1.0156	1.0194
Galerkin-tip	0.9549	0.9852	0.9951	1.0001	1.0030
PWLC	1.0967	1.1103	1.1153	1.1180	1.1198
PWLC-tip	1.0001	0.9921	0.9923	0.9930	0.9937
Exact	0.9682	0.9874	0.9937	0.9969	0.9987

Table 5.5: Stress intensity factors calculated using the asymptotic method.

asymptotic and energy formulations. The popular case of a pressurized crack with constant pressure, p_0, and total length $2L$ is considered. Since the stress intensity factor is given exactly by (2.24), all numerical results are stated in units of $p_0\sqrt{\pi L}$. Also, in addition to the methods listed in Table 5.1, the exact width at the PWCC nodal points is used (called Exact). This "method" is used to provide a reasonable indication of the accuracy obtainable with the particular stress intensity factor estimation scheme employed.

Asymptotic Method

For each of the width methods, the stress intensity factor is calculated from (3.15) using the nodal width magnitude corresponding to the nodal point closest to

the tip. Clearly accuracy depends on having small E_{tip} and being close to the crack tip. But, as mentioned elsewhere, not all methods have tip nodes the same distance from the crack tip. The results for the various width methods are presented in Table 5.5. The results essentially follow the tip accuracy trends encountered previously. However, it is clear that the one-term asymptotic method is limited to about a tenth of a percent relative error, for a reasonable number of elements. The most accurate methods are PWCC-tip-coll, Galerkin-tip and PWLC-tip.

Strain Energy Method

For each of the width methods, the stress intensity factor is calculated using (3.18). Since $p = p_0$, calculation of the strain energy is simplified. Strain energies are calculated using the midpoint rule for the PWCC and Exact methods, Galerkin methods use the weighting matrix approach, PWLC integrates the linear elements exactly, and PWLC-tip is like PWLC except that the tip element contribution is integrated exactly. Numerical results shown in Table 5.6 are generally more accurate than the asymptotic results. However, two matrix inversions are required in the energy method compared to only one in the asymptotic case. The most accurate methods are clearly PWCC-far-field and Galerkin-tip. A partial explanation for the less than spectacular PWLC-tip result is that the centred difference derivative approximation uses a step size of $2h$, instead of h, and therefore limits accuracy.

	Stress Intensity Factor (units of $p_0\sqrt{\pi L}$)				
	N				
	4	10	20	40	100
PWCC	1.030776	1.012423	1.006231	1.003120	1.001249
PWCC-tip	1.019838	1.007790	1.003856	1.001914	1.000760
PWCC-QGrid	0.993992	0.997600	0.998800	0.999400	0.999760
PWCC-far-field	1.000166	1.000065	1.000032	1.000016	1.000006
PWCC-tip-coll	1.005868	1.002349	1.001175	1.000588	1.000235
Galerkin	0.990800	0.995486	0.997555	0.998714	0.999463
Galerkin-tip	1.000063	0.999983	0.999989	0.999994	0.999998
PWLC	0.994618	0.996675	0.997915	0.998748	0.999389
PWLC-tip	0.999698	0.996063	0.997583	0.998580	0.999322
Exact	1.001754	1.000437	1.000154	1.000054	1.000014

Table 5.6: Stress intensity factors calculated using the strain energy method.

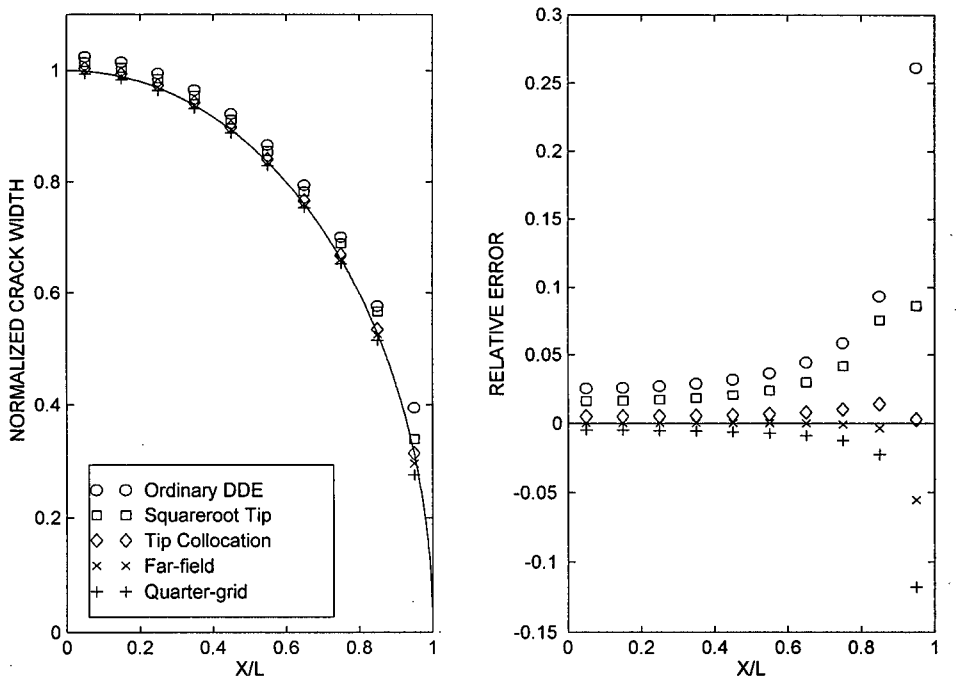

Figure 5.1: Plots of constant DD and related methods (N=10).

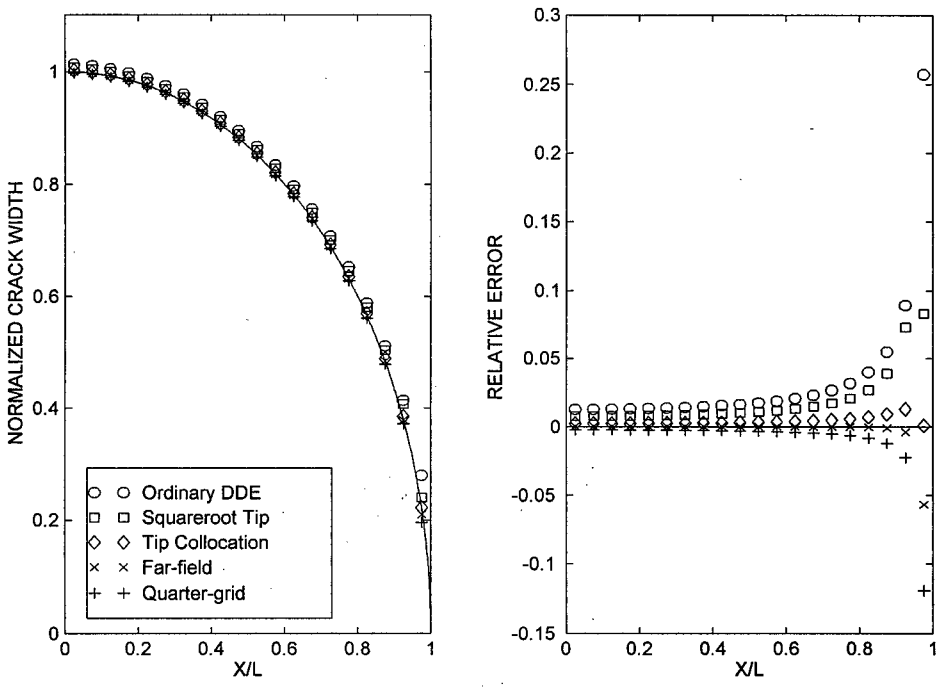

Figure 5.2: Plots of constant DD and related methods (N=20).

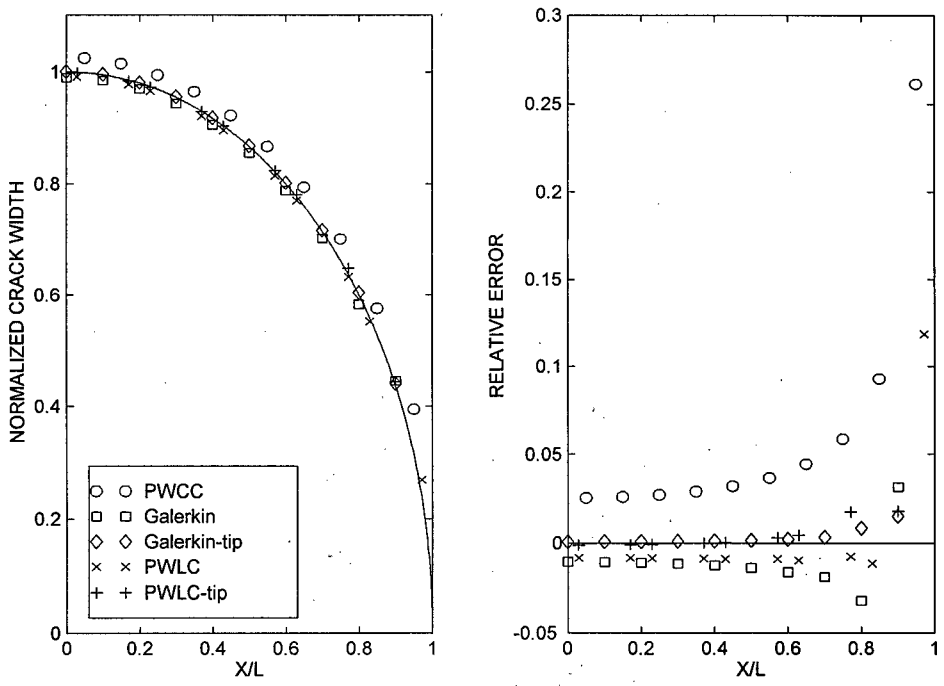

Figure 5.3: Plots of Galerkin and PWCL methods (N=10).

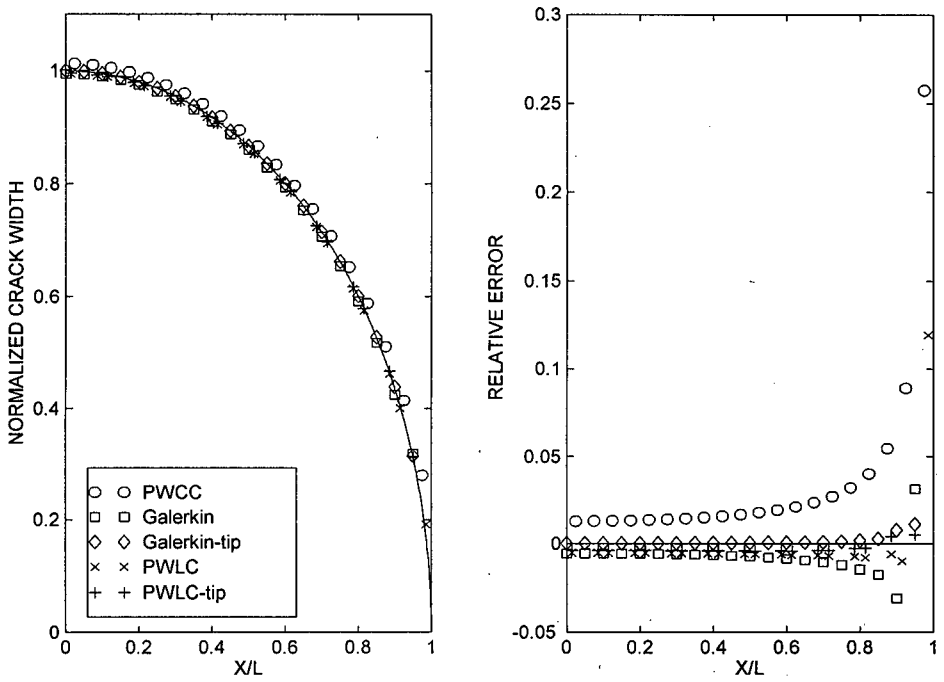

Figure 5.4: Plots of Galerkin and PWCL methods (N=20).

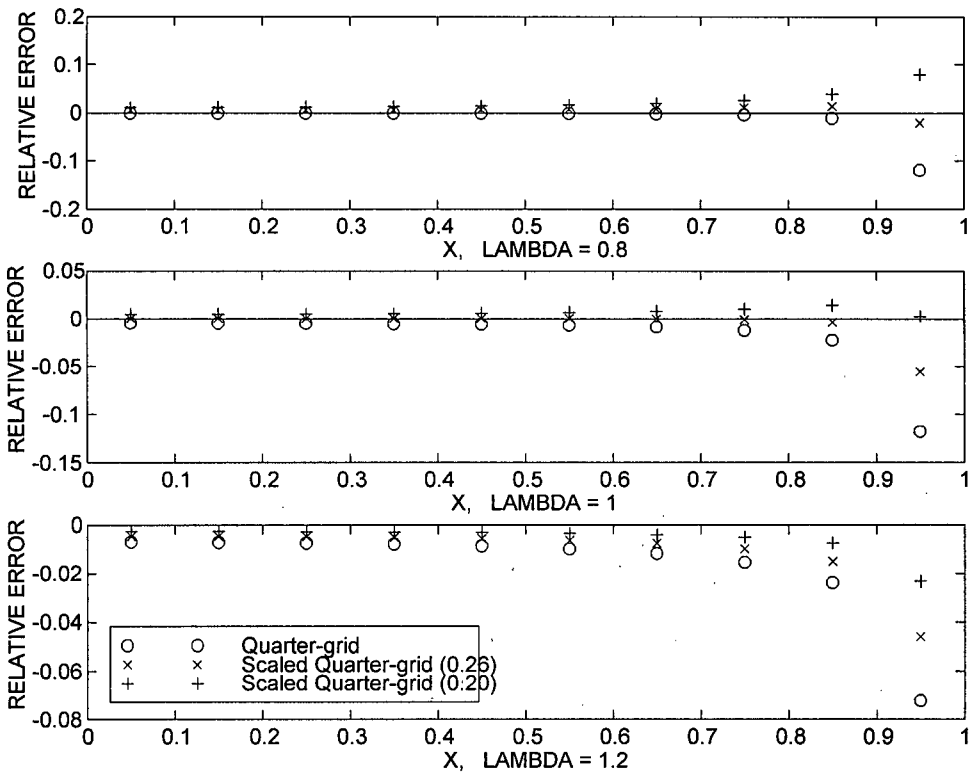

Figure 5.5: Quarter-grid and scaled variants (N=10).

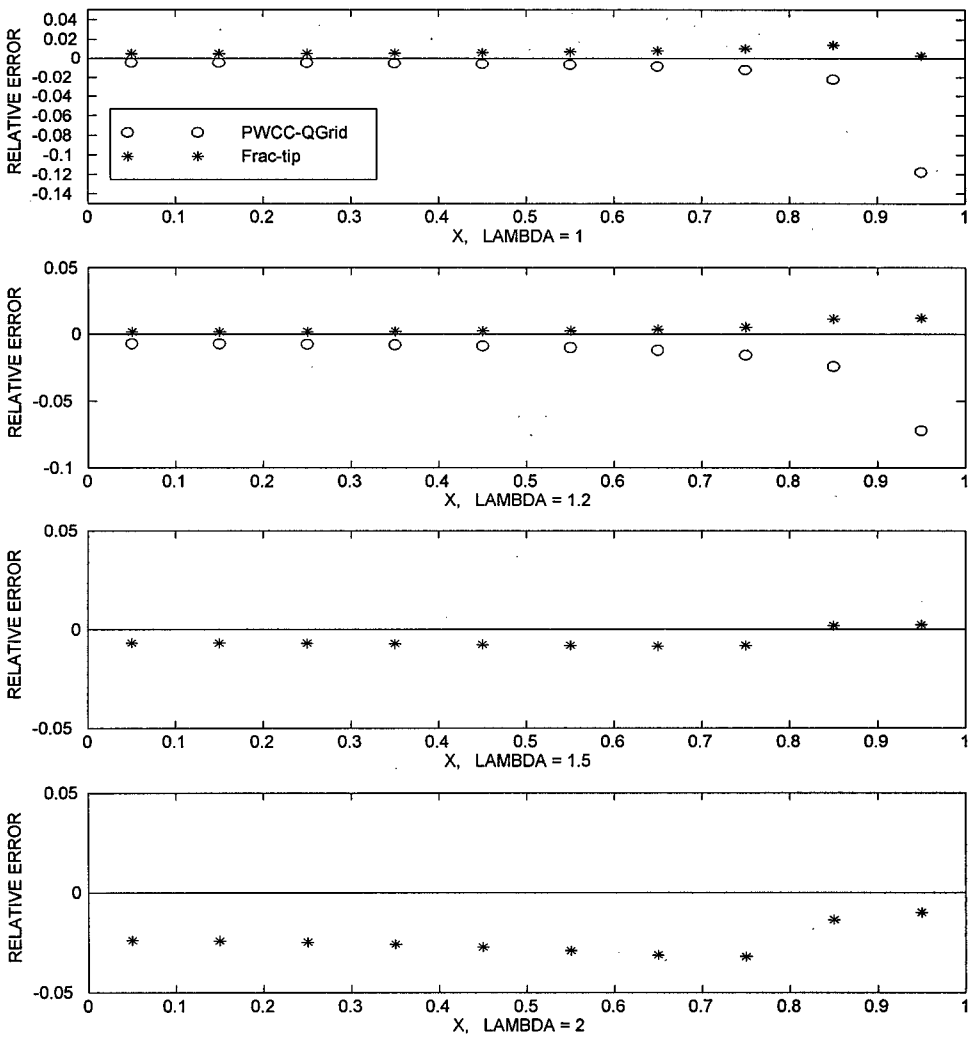

Figure 5.6: Fractional mining tip results (N=10).

Chapter 6

Conclusions

This research has addressed the comparison of DDM and Galerkin BEM for the pressurized line crack. The construction of various tip correction strategies for constant DDE on a grid of constant spacing was also addressed.

For the case of constant DD element discretization of a crack on a constant grid, numerical evidence has been found which suggests that various modifications of the crack tip element's self-effect have the ability to significantly reduce the crack width solution's error. This result was known previously, and a similar modification called the quarter-grid correction had been developed [27]. However, it has been found that other corrections yield comparable or better accuracy. Results indicate that increasing the self-effect by approximately 20% reduces the tip error significantly, while an increase of approximately 26% reduces the error near the middle of the crack. For comparison, the quarter-grid correction of Ryder and Napier suggests a one third increase in the self-effect. It appears that the correction strength is not strongly dependent of the number of DD elements or the pressure distribution. For example, in the case of the tip collocation method (20% correction), errors are less than half of those encountered using a squareroot tip element. It is hoped that the method may be generalized to more complicated problems and that benefits of the constant DD element crack problem formulation may be exploited with greater accuracy.

We attempted to generalize the self-effect correction method to the fractional mining problem. Rescaled quarter-grid-like corrections were constructed which corresponded to the 20% and 26% self-effect increases when there was no fractional mining. While the corrections produced results which had some favourable properties, it was found that relative errors in excess of 5% would have to be tolerated for all the methods. Certain scalings produced better errors for different length fractions, but only minor improvement was obtained overall.

An improved crack tip element correction was constructed for the constant DDE, constant grid spacing fractional mining problem. The method corrects not only the crack tip element's self-effect but also the tip element's stress influence on the adjacent element and vice versa. The correction allows the fractionally mined crack width to be calculated with errors generally much less than 3%. A notable point is that the tip error is never much larger than 1%.

The results of higher-order Galerkin and PWL collocation (PWLC) methods were also compared. It was found that the Galerkin and PWLC methods produced solutions with comparable accuracy. The tip corrected versions (Galerkin-tip and PWLC-tip) were also comparable in accuracy. However, there was a tendency for the tip-corrected Galerkin method to be extremely accurate in regions away from the crack tips, e.g., with 100 nodes, the relative error near the middle of the crack was a few 100 times less than comparable Galerkin, PWLC and tip-corrected PWLC results. In the absence of tip corrections, the PWLC method is essentially equivalent to the Galerkin method, on a constant grid of equal spacing, with the exception that the Galerkin method has slightly more accuracy at the crack tip.

Finally, the methods were also used to calculate stress intesity factors using asymptotic and strain energy release rate formulas. Methods that produced accurate crack width estimation near the crack tip, naturally produced the best stress inten-

sity factor approximations when using the asymptotic formula. The most accurate methods in that category were the tip collocation method (constant DDE with 20% self-effect increase) and both the Galerkin and PWLC methods with squareroot tip corrections. When the strain energy release rate formula was used, methods which produced the most accurate overall crack width were the most accurate. In this category, the Galerkin method with a squareroot tip correction was the most accurate, followed by the constant DDM with the 26% self-effect increase chosen to minimize the error near the middle of the crack.

Bibliography

[1] S. H. Advani, T. S. Lee and R. H. Dean, "Variational Principles for Hydraulic Fracturing," Journal of Applied Mechanics, 59, pp. 819-826, 1992.

[2] G. I. Barenblatt, "Mathematical Theory of Equilibrium Cracks," in *Advances in Applied Mechanics*, 7, pp. 55-129, 1962.

[3] R. S. Carbonell, "Self-Similar Solution of a Fluid-Driven Fracture", Ph.D. Thesis, University of Minnesota, 1996.

[4] R. J. Clifton and A. S. Abou-Sayed, On the Computation of the Three-Dimensional Geometry of Hydraulic Fractures, paper SPE 7943, 1979.

[5] A. M. Crawford and J. H. Curran, "Higher-order functional variation displacement discontinuity elements," Mech. Min. Sci. and Geomech. Abstr., 19, pp. 143-148.

[6] S. L. Crouch, Solution of plane elasticity problems by the displacement discontinuity method. *Int. J. Num. Methods Engng* 10, 301-43.

[7] S. L. Crouch, *Analysis of stresses and displacements around underground excavations: an application of the displacement discontinuity method.* Geomechanics report to the National Science Foundation. Minneapolis: University of Minnesota.

[8] S. L. Crouch and A. M. Starfield, *Boundary element methods in solid mechanics*, Cambridge, Unwin Hyman Inc., 1990.

[9] J. Desroches, E. Detournay, B. Lenoach, P. Papanastasiou, J. R. A. Pearson, M. Thiercelin and A. Cheng, "The crack tip region in hydraulic fracturing," Proc. R. Soc. London A, 447, pp. 39-48, 1994.

[10] J. Desroches and M. Thiercelin, "Modelling the Propagation and Closure of Micro-Hydraulic Fractures", Int. J. Rock Mech. Min. Sci. & Geomech. Abstr., 36, No. 7, pp. 1231-1234, 1993.

[11] A. H. England and A. E. Green, Some Two-dimensional Punch and Crack Problems in Classical Elasticity, *Proc. Cambridge Phil. Soc.*, London, 59, 489-500, 1963.

[12] A. D. Fitt, A. D. Kelly and C. P. Please, "Crack Propagation models for rock fracture in a geothermal energy reservoir," SIAM J. Appl. Math., 55, No. 6, pp. 1592-1608, 1995.

[13] L. B. Freund, *Dynamic Fracture Mechanics*, Cambridge University Press, New York, 1990.

[14] J. Geertsma and F. de Klerk, "A Rapid Method of Predicting Width and Extent of Hydraulically Induced Fractures," Journal of Petroleum Technology, pp. 1571-1581, December 1969.

[15] A. E. Green and W. Zerna, *Theoretical Elasticity*, Oxford University Press, London, 1968.

[16] A. A. Griffith, The Phenomena of Rupture and Flow in Solids, Phil. Trans. Royal Soc. London, Ser. A. 221, 163-198, 1920.

[17] A. A. Griffith, The Theory of Rupture, Proc. First international Congress on Applied Mechanics, Delft, 55-63, 1924.

[18] M. F. Kanninen and C. H. Popelar, *Advanced Fracture Mechanics*, Oxford University Press, New York, 1985.

[19] S. A. Kristianovitch and Y. P. Zheltov, Formation of Vertical Fractures by Means of Highly Viscous Fluids, *Proc. World Pet. Cong.*, Rome, 2, 579, 1955.

[20] N. I. Muskhelishvili, *Some Basic Problems of the Mathematical Theory of Elasticity; Fundamental Equations, Plane Theory of Elasticity, Torsion and Bending*, 5th ed., Noordhoff, Gröningen, Leyden, The Netherlands, 1953.

[21] J. A. L. Napier, Personal communication, 1997.

[22] V. Z. Parton and E. M. Morozov, *Elastic-Plastic Fracture Mechanics*, Mir, Moscow, 1978.

[23] R. P. Nordgren, "Propagation of a Vertical Hydraulic Fracture," Society of Petroleum Engineers Journal, pp. 306-314, August 1972.

[24] T. K. Perkins and L. R. Kern, "Widths of Hydraulic Fractures," Journal of Petroleum Technology, pp. 937-949, September 1961.

[25] S. T. Raveendra and T. A. Cruse, "BEM Analysis of Problems of Fracture Mechanics," in *Developments in Boundary Element Methods - 5: Industrial Applications of Boundary Element Methods*, P. K. Banerjee and R. B. Wilson (ed.), Elsevier Science, New York, pp. 187-204, 1989.

[26] J. R. Rice, "Mathematical Analysis in the Mechanics of Fracture," in *Fracture*, H. Leibovitz (ed.), Vol. 2, Academic Press, New York, 1968.

[27] J. A. Ryder and J. A. L. Napier, "Error analysis and design of a large-scale tabular mining stress analyser," Proceedings of the fifth international conference on numerical methods in geomechanics, Nagoya, pp. 1549-1555, 1985.

[28] The SCR Geomechanics Group, "On the Modelling of Near Tip Processes in Hydraulic Fractures," Ing. J. Rock Mech. Min. Sci. & Geomech. Abstr., 7, pp. 1127-1134, 1993.

[29] R. A. Schmidt, A microcrack model and its significance to hydraulic fracturing and fracture toughness testing, *Proc. 21st US Symp. on Rock Mech.*, pp. 581-590.

[30] I. N. Sneddon, *Elements of Partial Differential Equations*, McGraw-Hill, New York, 1957.

[31] I. N. Sneddon, *Integral Transform Methods, in Mechanics of Fracture I, Methods of analysis and solutions of crack problems*, G. C. Sih (ed.), Nordhoff International, Leyden, 1973.

[32] I. S. Sokolnikoff, *Mathematical Theory of Elasticity*, pp. 179-180, McGraw-Hill, New York, 1956.

[33] D. A. Spence and P. Sharp, "Self-similar solutions for elastohydrodynamic cavity flow," Proc. R. Soc. London A, 400, pp. 289-313, 1985.

[34] S. P. Timoshenko and J. N. Goodier, *Theory of Elasticity*, 3rd. ed., McGraw-Hill, New York, 1970.

[35] D. J. Unger, *Analytical Fracture Mechanics*, London, Academic Press, Inc., 1995

[36] P. Valkó and M. J. Economides, *Hydraulic Fracture Mechanics*, New York, John Wiley and Sons, Inc., 1995.

[37] B. N. Whittaker, R. N. Singh and G. Sun, *Rock Fracture Mechanics: Principles, Design and Applications*, Elsevier Science Publishers, New York, 1992.

[38] Y. P. Zheltov and S. A. Kristianovitch, On the Mechanism of Hydraulic Fracture of an Oil-Bearing Stratum, *Izv. AN SSSR*, OTN, (No. 5), 3-41, 1955.

Appendices

A. Stresses and Displacements for a DD of Finite Length

This Appendix restates the results given by Crawford and Curran [5] with due reference to Crouch [6].

Consider a general DDE in the xy-plane of length $2a$, located along the x-axis from $-a$ to a. Assume, as usual, that the elastic medium is linear, homogeneous and isotropic. If the normal and shear displacements of the DD are given by $D_N(x)$ and $D_S(x)$, respectively, then all stresses and displacements in the medium can be explicitly defined. Defining

$$\begin{aligned} \frac{\partial f(x,y)}{\partial x} &= \frac{1}{4\pi(1-\nu)} \frac{x}{x^2+y^2} \\ \frac{\partial f(x,y)}{\partial y} &= \frac{1}{4\pi(1-\nu)} \frac{y}{x^2+y^2} \end{aligned}$$

the normal and shear DD contributions to the stress and displacement fields are given by the following expressions.

Normal Displacement Discontinuity, $D_N(\varepsilon)$

$$\begin{aligned} u_x &= \left[(1-2\nu) + y\frac{\partial}{\partial y}\right] \int_{-a}^{a} \frac{\partial f(x-\varepsilon,y)}{\partial x} D_N(\varepsilon)d\varepsilon \\ u_y &= \left[-2(1-\nu) + y\frac{\partial}{\partial y}\right] \int_{-a}^{a} \frac{\partial f(x-\varepsilon,y)}{\partial y} D_N(\varepsilon)d\varepsilon \\ \sigma_{xx} &= 2G\left[\frac{\partial}{\partial y} + y\frac{\partial^2}{\partial y^2}\right] \int_{-a}^{a} \frac{\partial f(x-\varepsilon,y)}{\partial y} D_N(\varepsilon)d\varepsilon \\ \sigma_{yy} &= 2G\left[\frac{\partial}{\partial y} - y\frac{\partial^2}{\partial y^2}\right] \int_{-a}^{a} \frac{\partial f(x-\varepsilon,y)}{\partial y} D_N(\varepsilon)d\varepsilon \end{aligned}$$

$$\sigma_{xy} = 2G\left[-y\frac{\partial^2}{\partial y^2}\right]\int_{-a}^{a}\frac{\partial f(x-\varepsilon,y)}{\partial x}D_N(\varepsilon)d\varepsilon$$

Shear Displacement Discontinuity, $D_S(\varepsilon)$

$$\begin{aligned}
u_x &= -2(1-\nu)\int_{-a}^{a}\frac{\partial f(x-\varepsilon,y)}{\partial y}D_S(\varepsilon)d\varepsilon \\
&\quad +y\frac{\partial}{\partial x}\int_{-a}^{a}\frac{\partial f(x-\varepsilon,y)}{\partial x}D_S(\varepsilon)d\varepsilon \\
u_y &= -(1-2\nu)\int_{-a}^{a}\frac{\partial f(x-\varepsilon,y)}{\partial x}D_S(\varepsilon)d\varepsilon \\
&\quad +y\frac{\partial}{\partial y}\int_{-a}^{a}\frac{\partial f(x-\varepsilon,y)}{\partial x}D_S(\varepsilon)d\varepsilon \\
\sigma_{xx} &= 2G\left[2\frac{\partial}{\partial y}+y\frac{\partial^2}{\partial y^2}\right]\int_{-a}^{a}\frac{\partial f(x-\varepsilon,y)}{\partial x}D_S(\varepsilon)d\varepsilon \\
\sigma_{yy} &= 2G\left[-y\frac{\partial^2}{\partial y^2}\right]\int_{-a}^{a}\frac{\partial f(x-\varepsilon,y)}{\partial x}D_S(\varepsilon)d\varepsilon \\
\sigma_{xy} &= 2G\left[\frac{\partial}{\partial y}+y\frac{\partial^2}{\partial y^2}\right]\int_{-a}^{a}\frac{\partial f(x-\varepsilon,y)}{\partial y}D_S(\varepsilon)d\varepsilon
\end{aligned}$$

B. Influence Matrix Simplification for the Symmetric Problem

Assume that N is even, $p(x) = p(-x)$, and that the DDE nodal points are symmetrically located about $x = 0$, namely $x_k = -x_{N-k+1}$. In this case, the symmetry of the problem implies that the DDE solution with also be symmetric about $x = 0$, i.e., $D_y^k = D_y^{N-k+1}$. Let $N = 2M$. Expressing (3.12) as

$$-p_k = \sum_{j=1}^{M} A_{k,j}D_y^j + \sum_{j=1}^{M} A_{k,M+j}D_y^{M+j}, \qquad k = 1,...,M, \tag{B.1}$$

$$-p_{M+k} = \sum_{j=1}^{M} A_{M+k,j}D_y^j + \sum_{j=1}^{M} A_{M+k,M+j}D_y^{M+j}, \qquad k = 1,...,M, \tag{B.2}$$

use the fact that $p_k = p_{M+(M+1-k)}$ to rewrite (B.2) as

$$-p_k = -p_{2M+1-k} = \sum_{j=1}^{M} A_{2M+1-k,j}D_y^j + \sum_{j=1}^{M} A_{2M+1-k,M+j}D_y^{M+j}, \qquad k = 1,...,M. \tag{B.3}$$

Adding (B.1) and (B.3) yields

$$-2p_k = \sum_{j=1}^{M}\left(A_{k,j} + A_{2M+1-k,j}\right)D_y^j + \sum_{j=1}^{M}\left(A_{k,M+j} + A_{2M+1-k,M+j}\right)D_y^{M+j}. \tag{B.4}$$

Then, express (B.4) in terms of p_{M+k} and D_y^{M+j}:

$$\begin{aligned} -p_{M+k} &= \frac{1}{2}\sum_{j=1}^{M}\left(A_{M+k,j}+A_{M+1-k,j}\right)D_y^j+\frac{1}{2}\sum_{j=1}^{M}\left(A_{M+k,M+j}+A_{M+1-k,M+j}\right)D_y^{M+j} \\ &= \frac{1}{2}\sum_{J=1}^{M}\left(A_{M+k,M+1-J}+A_{M+1-k,M+1-J}\right)D_y^{M+1-J}+ \\ &\quad \frac{1}{2}\sum_{j=1}^{M}\left(A_{M+k,M+j}+A_{M+1-k,M+j}\right)D_y^{M+j} \\ &= \frac{1}{2}\sum_{J=1}^{M}\left(A_{M+k,M+1-J}+A_{M+1-k,M+1-J}\right)D_y^{M+J}+ \\ &\quad \frac{1}{2}\sum_{j=1}^{M}\left(A_{M+k,M+j}+A_{M+1-k,M+j}\right)D_y^{M+j} \end{aligned}$$

where the fact that $D_y^k = D_y^{N+1-k}$ was used. Finally, this can be written as

$$-\hat{p}_k = \sum_{j=1}^{M} B_{kj}\hat{D}_y^j \tag{B.5}$$

where

$$B_{kj} = \frac{1}{2}\left(A_{M+k,M+j}+A_{M+1-k,M+j}+A_{M+k,M+1-j}+A_{M+1-k,M+1-j}\right) \tag{B.6}$$

is the influence matrix for the positive interval and the circumflex indicates quantities on the positive x-axis, e.g., $p_{M+k} = \hat{p}_k$. Note that this approach works for appropriate non-DDM as well.

C. PWLC Matrices

This section details the construction of the matrix equation for the piecewise linear collocation (PWLC) method.

Consider a line crack from $x = -L$ to $x = L$ discretized with $2N$ PWL DDE of equal length $h = 2a = \frac{L}{N}$. Therefore the line crack has $4N$ nodal points along the crack. Using Gauss-Chebyshev collocation point positioning, the nodes are located at

$$x_k = -L + a\left[k - \frac{1}{2} + (-1)^k\left(\frac{\sqrt{2}-1}{2}\right)\right], \qquad k = 1, 2, ..., 4N,$$

so that

$$-L < x_1 < x_2 < \cdots < x_{2N} < 0 < x_{2N+1} < \cdots < x_{4N-1} < x_{4N} < L.$$

Using (3.25), the normal stress at the j^{th} node is

$$\sigma_j = \sigma_{yy}(x_j, 0) = \frac{G}{2\pi(1-\nu)} \sum_{m=1}^{2N} [F(x_{jm}, -1)D_1^m + F(x_{jm}, +1)D_2^m]$$

where D_1^m and D_2^m are the nodal displacements of the m^{th} DDE and

$$x_{jm} = x_j - (\text{centre of } m^{\text{th}} \text{ DDE}).$$

Letting d_k be the nodal displacement corresponding to the node located at x_k, then the resulting $4N \times 4N$ matrix equation is

$$\sigma_j = \sum_{k=1}^{4N} A_{jk} d_k$$

where

$$\begin{aligned} A_{jk} &= \frac{G}{2\pi(1-\nu)} F(x_{jk}, (-1)^k) \\ &= \frac{G}{2\pi(1-\nu)} \left\{ \frac{a}{x_{jk}^2 - a^2} + (-1)^k \sqrt{2} \left[\frac{x_{jk}}{x_{jk}^2 - a^2} + \frac{1}{2a} \ln \left| \frac{x_{jk} - a}{x_{jk} + a} \right| \right] \right\} \end{aligned}$$

and x_{jk} is the signed distance from x_j to the centre of the element with a node at x_k:

$$x_{jk} = x_j - \bar{x}_k$$

and

$$\bar{x}_k = -L + \frac{a}{2} \left[2k - 1 + (-1)^{k+1} \right]$$

Also, for the symmetric pressurized crack problem, the $4N \times 4N$ matrix equation may be converted to a $2N \times 2N$ equation using the simple procedure given in Appendix B.

D. Galerkin Matrices using PWL Basis Functions

This section concerns the calculation of the stress and weighting matrices, S_{nm} and M_{nm} respectively.

Stress Matrix, S_{nm}

In order to calculate the stress matrix, S_{nm}, given by (4.11), the derivatives of the PWL basis functions $\phi_n(x)$, defined by (4.4) and (4.5), are found to be

$$\frac{d\phi_n(x)}{dx} = \begin{cases} m_{n-1}, & x \in \Lambda_{n-1}, \\ -m_n, & x \in \Lambda_n, \\ 0, & \textbf{otherwise}, \end{cases}$$

where $\Lambda_n = \{x | x \in (x_k, x_{k+1})\}$. Therefore, the stress matrix is

$$\begin{aligned} S_{nm} &= \frac{E'}{4\pi}\int_0^L dx' \int_0^L dx \ln\left|\frac{x+x'}{x-x'}\right| \frac{d\phi_n(x')}{dx'}\frac{d\phi_m(x)}{dx} \\ &= \frac{E'}{4\pi}\int_{\Lambda_{n-1}+\Lambda_n} dx' \int_{\Lambda_{m-1}+\Lambda_m} dx \ln\left|\frac{x+x'}{x-x'}\right| \frac{d\phi_n(x')}{dx'}\frac{d\phi_m(x)}{dx} \\ &= \frac{E'}{4\pi}\left\{ m_{n-1}m_{m-1}\int_{\Lambda_{n-1}} dx' \int_{\Lambda_{m-1}} dx - m_{n-1}m_m \int_{\Lambda_{n-1}} dx' \int_{\Lambda_m} dx \right. \\ &\qquad \left. -m_n m_{m-1}\int_{\Lambda_n} dx' \int_{\Lambda_{m-1}} dx + m_n m_m \int_{\Lambda_n} dx' \int_{\Lambda_m} dx \right\} \ln\left|\frac{x+x'}{x-x'}\right| \\ &= \frac{E'}{4\pi}\{m_{n-1}m_{m-1}C_{n-1,m-1} - m_{n-1}m_m C_{n-1,m} - m_n m_{m-1}C_{n,m-1} \\ &\qquad + m_n m_m C_{n,m}\} \end{aligned}$$

where

$$C_{n,m} = C_{m,n} = \int_{\Lambda_n} dx' \int_{\Lambda_m} dx \ln\left|\frac{x+x'}{x-x'}\right|, \qquad n, m = 1, 2, ..., N$$

and

$$C_{0,m} = C_{m,0} = 0, \qquad m = 0, 1, ..., N.$$

By changing variables with

$$x' = x_n + (x_{n+1} - x_n)\eta'$$

$$x = x_m + (x_{m+1} - x_m)\eta$$

then

$$\begin{aligned} C_{n,m} &= \int_{\Lambda_n} dx' \int_{\Lambda_m} dx \ln\left|\frac{x+x'}{x-x'}\right| \\ &= (x_{n+1}-x_n)(x_{m+1}-x_m)\int_0^1 d\eta' \int_0^1 d\eta \ln\left|\frac{a_{nm}+c_{nm}\eta+\eta'}{b_{nm}+c_{nm}\eta-\eta'}\right| \end{aligned}$$

where

$$\begin{aligned} a_{nm} &= \frac{x_n + x_m}{x_{n+1}-x_n}, \\ b_{nm} &= \frac{x_m - x_n}{x_{n+1}-x_n}, \\ c_{nm} &= \frac{x_{m+1}-x_m}{x_{n+1}-x_n}. \end{aligned}$$

There are three cases to be considered if the symmetry condition, $C_{n,m} = C_{m,n}$, is used.

Case I *($m = n$)*: **When $n = m$,**

$$\begin{aligned} a_{nn} &= \frac{2x_n}{x_{n+1}-x_n} > 0, \\ b_{nn} &= 0, \\ c_{nn} &= 1, \end{aligned}$$

and $C_{n,n}$ simplifies to

$$\frac{(a_{nn})^2 \ln a_{nn}}{2} + (a_{nn}+1)^2 \ln\left(\frac{\sqrt{a_{nn}+2}}{a_{nn}+1}\right) + (2a_{nn}+3)\ln\sqrt{a_{nn}+2}$$

$$\begin{aligned} C_{n,n} &= (x_{n+1}-x_n)^2 \int_0^1 d\eta' \int_0^1 d\eta \ln\left|\frac{a_{nn}+\eta+\eta'}{\eta-\eta'}\right| \\ &= (x_{n+1}-x_n)^2 \left\{ \frac{(a_{nn})^2 \ln a_{nn}}{2} + (a_{nn}+1)^2 \ln\left(\frac{\sqrt{a_{nn}+2}}{a_{nn}+1}\right) \right. \\ &\quad \left. +(2a_{nn}+3)\ln\sqrt{a_{nn}+2}\right\} \end{aligned}$$

Case II *($m = n+1$)*: **In this case,**

$$a_{nm} = \frac{x_n + x_m}{x_{n+1}-x_n} > 0,$$

$$\begin{aligned} b_{nm} &= 1, \\ c_{nm} &= \frac{x_{m+1}-x_m}{x_{n+1}-x_n} > 0, \end{aligned}$$

and therefore

$$C_{n,m} = (x_{n+1}-x_n)(x_{m+1}-x_m)\int_0^1 d\eta' \int_0^1 d\eta \ln\left|\frac{a_{nm}+c_{nm}\eta+\eta'}{1+c_{nm}\eta-\eta'}\right|$$

may be integrated to yield

$$\begin{aligned} C_{n,n+1} &= \frac{1}{2}(x_{n+1}-x_n)^2\left\{(a+c)^2\ln(1+(a+c)^{-1}) + (1+2(a+c))\ln(1+a+c)\right. \\ &\quad \left. -(1+a)^2\ln(1+a) - (1+c)^2\ln(1+c) + a^2\ln a + c^2\ln c\right\} \end{aligned}$$

where $a = a_{n,n+1}$ **and** $c = c_{n,n+1}$.

Case III ($m > n+1$)**: This case requires the most general integration. However, using the fact that** $b_{nm} > 1$,

$$\begin{aligned} C_{\substack{n,m \\ m>n+1}} &= (x_{n+1}-x_n)(x_{m+1}-x_m)\int_0^1 d\eta' \int_0^1 d\eta \ln\left|\frac{a_{nm}+c_{nm}\eta+\eta'}{b_{nm}+c_{nm}\eta-\eta'}\right| \\ &= \frac{1}{2}(x_{n+1}-x_n)^2\left\{(a+c)^2\ln(1+(a+c)^{-1}) + (1+2(a+c))\ln(1+a+c)\right. \\ &\quad +(b+c-1)^2\ln(b+c-1) - (b+c)^2\ln(b+c) - (b-1)^2\ln(b-1) \\ &\quad \left. -(1+a)^2\ln(1+a) + b^2\ln b + a^2\ln a\right\} \end{aligned}$$

where $a = a_{nm}$, $b = b_{nm}$ **and** $c = c_{nm}$.

Weighting Matrix, M_{nm}

The weighting matrix, M_{nm}**, is given by (4.10) for the case of PWL basis functions. This may be simplified using (4.4) and (4.5):**

$$\begin{aligned} M_{nm} &= \delta_{nm}\int_0^L \phi_n(x)dx \\ &= \delta_{nm}\left\{\int_{\Lambda_{n-1}} [m_{n-1}(x-x_{n-1})+\delta_{n1}]\,dx + \int_{\Lambda_n} m_n(x_{n+1}-x)dx\right\} \\ &= \delta_{nm}\left\{(1-\delta_{n1})\frac{x_n-x_{n-1}}{2} + \delta_{n1}(x_n-x_{n-1}) + \frac{x_{n+1}-x_n}{2}\right\} \\ &= \frac{\delta_{nm}}{2}\{x_{n+1}-x_{n-1}+\delta_{n1}x_n\} \end{aligned}$$

E. Galerkin Matrices using Tip-corrected PWL Basis Functions

This section concerns the calculation of the stress and weighting matrices, $\hat{S}_{nm}$ and $\hat{M}_{nm}$, in the case that the tip-corrected PWL basis functions, $\{\hat{\phi}_k\}_{k=1}^N$, are used.

Stress Matrix, $\hat{S}_{nm}$

Since the $\hat{\phi}_k$ basis functions are identical to the ϕ_k except for the $j = N$ case, the stiffness matrix,

$$\hat{S}_{nm} = \frac{E'}{4\pi}\int_0^L dx' \int_0^L dx \ln\left|\frac{x+x'}{x-x'}\right| \frac{d\hat{\phi}_n(x')}{dx'}\frac{d\hat{\phi}_m(x)}{dx},$$

will be identical to S_{nm} for $n, m \neq N$. Also, since $\hat{S}_{nm}$ is symmetric, it will be sufficient to calculate the $m = N$ column for $n = 1, 2, ..., N$.

From (4.6) and (4.7), the derivatives of the basis functions are

$$\frac{d\hat{\phi}_n(x)}{dx} = \begin{cases} m_{n-1}, & x \in \Lambda_{n-1} \\ -m_n, & x \in \Lambda_n \\ 0, & \textbf{otherwise,} \end{cases}, \qquad n = 1, 2, ..., N-1,$$

and

$$\frac{d\hat{\phi}_N(x)}{dx} = \begin{cases} m_{N-1}, & x \in \Lambda_{N-1} \\ -\frac{1}{2}m_N\sqrt{\frac{L-x_N}{L-x}}, & x \in \Lambda_N \\ 0, & \textbf{otherwise,} \end{cases}.$$

Substitution into the $\hat{S}_{nm}$ expression, when $n < N$ and $m = N$, yields

$$\begin{aligned} \hat{S}_{nN} &= \frac{E'}{4\pi}\int_0^L dx' \int_0^L dx \ln\left|\frac{x+x'}{x-x'}\right| \frac{d\hat{\phi}_n(x')}{dx'}\frac{d\hat{\phi}_N(x)}{dx} \\ &= \frac{E'}{4\pi}\int_{\Lambda_{n-1}+\Lambda_n} dx' \int_{\Lambda_{N-1}+\Lambda_N} dx \ln\left|\frac{x+x'}{x-x'}\right| \frac{d\hat{\phi}_n(x')}{dx'}\frac{d\hat{\phi}_N(x)}{dx} \\ &= \frac{E'}{4\pi}\Big\{m_{n-1}m_{N-1}C_{n-1,N-1} - m_{n-1}m_N\hat{C}_{n-1,N} - m_n m_{N-1}C_{n,N-1} \\ &\qquad + m_n m_N \hat{C}_{n,N}\Big\} \end{aligned}$$

where $C_{n,m}$ is as before and

$$\hat{C}_{n,N} = \hat{C}_{N,n} = \frac{1}{2}\int_{\Lambda_n} dx' \int_{\Lambda_N} dx \sqrt{\frac{L-x_N}{L-x}} \ln\left|\frac{x+x'}{x-x'}\right|.$$

In the case $n = m = N$,

$$\hat{S}_{NN} = \frac{E'}{4\pi}\left\{m_{N-1}m_{N-1}C_{N-1,N-1} - 2m_{N-1}m_N\hat{C}_{N-1,N} + m_N m_N \bar{C}_{N,N}\right\},$$

where

$$\bar{C}_{N,N} = \frac{1}{4}\int_{\Lambda_N} dx' \int_{\Lambda_N} dx \frac{L-x_N}{\sqrt{(L-x')(X-x)}} \ln\left|\frac{x+x'}{x-x'}\right|.$$

The $\hat{C}_{n,N}$ integral may be solved. Changing variables and separating the logarithm,

$$\begin{aligned}\hat{C}_{n,N} &= \frac{(x_{n+1}-x_n)(L-x_N)}{2}\int_0^1 d\eta' \int_0^1 d\eta (1-\eta)^{-\frac{1}{2}} \ln\left|\frac{a_{nN}+c_{nN}\eta+\eta'}{b_{nN}+c_{nN}\eta-\eta'}\right| \\ &= \frac{(x_{n+1}-x_n)(L-x_N)}{2}\left\{N_{n,N} - D_{n,N}\right\},\end{aligned}$$

where a_{nN}, b_{nN} and c_{nN} are the same as in the previous section and

$$\begin{aligned}N_{n,N} &= \int_0^1 d\eta' \int_0^1 d\eta (1-\eta)^{-\frac{1}{2}} \ln\left(a_{nN}+c_{nN}\eta+\eta'\right) \\ D_{n,N} &= \int_0^1 d\eta' \int_0^1 d\eta (1-\eta)^{-\frac{1}{2}} \ln\left|b_{nN}+c_{nN}\eta-\eta'\right|\end{aligned}$$

It follows that

$$\begin{aligned}N_{n,N} &= \frac{2}{3}\left\{4c\left[\left(\frac{1+a+c}{c}\right)^{\frac{3}{2}}\tanh^{-1}\sqrt{\frac{c}{1+a+c}} - \left(\frac{a+c}{c}\right)^{\frac{3}{2}}\tanh^{-1}\sqrt{\frac{c}{a+c}}\right]\right. \\ &\quad \left.+(3a+2c)\ln\left(\frac{1+a}{a}\right) + 3\ln(1+a) - 7\right\},\end{aligned}$$

and

$$\begin{aligned}D_{\substack{n,N \\ n<N-1}} &= -\frac{2}{3}\left\{4c\left[\left(\frac{b+a-1}{c}\right)^{\frac{3}{2}}\tanh^{-1}\sqrt{\frac{c}{b+c-1}} - \left(\frac{b+c}{c}\right)^{\frac{3}{2}}\tanh^{-1}\sqrt{\frac{c}{b+c}}\right]\right. \\ &\quad \left.+(3b+2c)\ln\left(\frac{b-1}{b}\right) - 3\ln(b-1) + 7\right\}, \\ D_{N-1,N} &= -\frac{14}{3} + 4\sqrt{3}\tanh^{-1}\left(\frac{1}{\sqrt{3}}\right) - \frac{2}{3}\ln 2.\end{aligned}$$

where $a = a_{nN}$, $b = b_{nN}$ and $c = c_{nN}$ are shortened notations.

While the $\bar{C}_{N,N}$ integral has not been solved exactly, it may be simply approximated. Introducing a change of variables,

$$\begin{aligned}\bar{C}_{N,N} &= \frac{1}{4}\int_{\Lambda_N} dx' \int_{\Lambda_N} dx \frac{L - x_N}{\sqrt{(L-x')(X-x)}} \ln\left|\frac{x+x'}{x-x'}\right| \\ &= \frac{(L-x_N)^2}{4}\int_0^1 d\eta' \int_0^1 d\eta \left[(1-\eta')(1-\eta)\right]^{-\frac{1}{2}} \ln\left[\frac{a_{NN}+\eta+\eta'}{|\eta-\eta'|}\right],\end{aligned}$$

where

$$a_{NN} = \frac{2x_N}{L - x_N}.$$

Notice that $a_{NN} \gg 1$ when $N \gg 1$. Rewriting the $\bar{C}_{N,N}$ integral as

$$\begin{aligned}\bar{C}_{N,N} &= \frac{(L-x_N)^2}{4}\int_0^1 d\eta' \int_0^1 d\eta \left[(1-\eta')(1-\eta)\right]^{-\frac{1}{2}} \\ &\quad \left\{\ln\left[1 + \frac{\eta+\eta'}{a_{NN}}\right] + \ln a_{NN} - \ln|\eta-\eta'|\right\} \\ &= \frac{(L-x_N)^2}{4}\left\{\Gamma_1 + \Gamma_2 - \Gamma_3\right\}\end{aligned}$$

with

$$\begin{aligned}\Gamma_1 &= \int_0^1 d\eta' \int_0^1 d\eta \left[(1-\eta')(1-\eta)\right]^{-\frac{1}{2}} \ln\left[1 + \frac{\eta+\eta'}{a_{NN}}\right], \\ \Gamma_2 &= \int_0^1 d\eta' \int_0^1 d\eta \left[(1-\eta')(1-\eta)\right]^{-\frac{1}{2}} \ln a_{NN}, \\ \Gamma_3 &= \int_0^1 d\eta' \int_0^1 d\eta \left[(1-\eta')(1-\eta)\right]^{-\frac{1}{2}} \ln|\eta-\eta'|\end{aligned}$$

straightforward integration yields

$$\Gamma_2 = 4\ln a_{NN}$$

and

$$\Gamma_3 = 8\ln 2 - 12.$$

Using the expansion

$$\ln(1+x) = x - \frac{1}{2}x^2 + \frac{1}{3}x^3 - \frac{1}{4}x^4 + \frac{1}{5}x^5 - \ldots$$

in the integrand of the Γ_1 integral, an approximation can be generated for large a_{NN}:

$$\begin{aligned}\Gamma_1 &= \frac{16}{3}a_{NN}^{-1} - \frac{176}{45}a_{NN}^{-2} + \frac{256}{63}a_{NN}^{-3} - \frac{7808}{1575}a_{NN}^{-4} + \\ &\quad \frac{346112}{51975}a_{NN}^{-5} - \frac{9029632}{945945}a_{NN}^{-6} + \frac{1507328}{105105}a_{NN}^{-7} + O\left(a_{NN}^{-8}\right).\end{aligned}$$

In practice, it was found that seven terms of the series were sufficient to approximate Γ_1 to six significant figures, assuming a constant grid and $N \geq 5$.

Weighting Matrix, $\hat{M}_{nm}$

The diagonal weighting matrix, $\hat{M}_{nm}$, corresponding to the $\hat{\phi}_k$ basis functions, is identical to M_{nm} for $n < N$. The $\hat{M}_{NN}$ element is given by

$$\begin{aligned}\hat{M}_{NN} &= \int_0^L \hat{\phi}_N(x)dx \\ &= \int_{\Lambda_{N-1}} \left(\frac{x - x_{N-1}}{x_N - x_{N-1}}\right) dx + \int_{\Lambda_N} \sqrt{\frac{L-x}{L-x_N}}dx \\ &= \frac{x_N - x_{N-1}}{2} + \frac{2}{3}(L - x_N)\end{aligned}$$